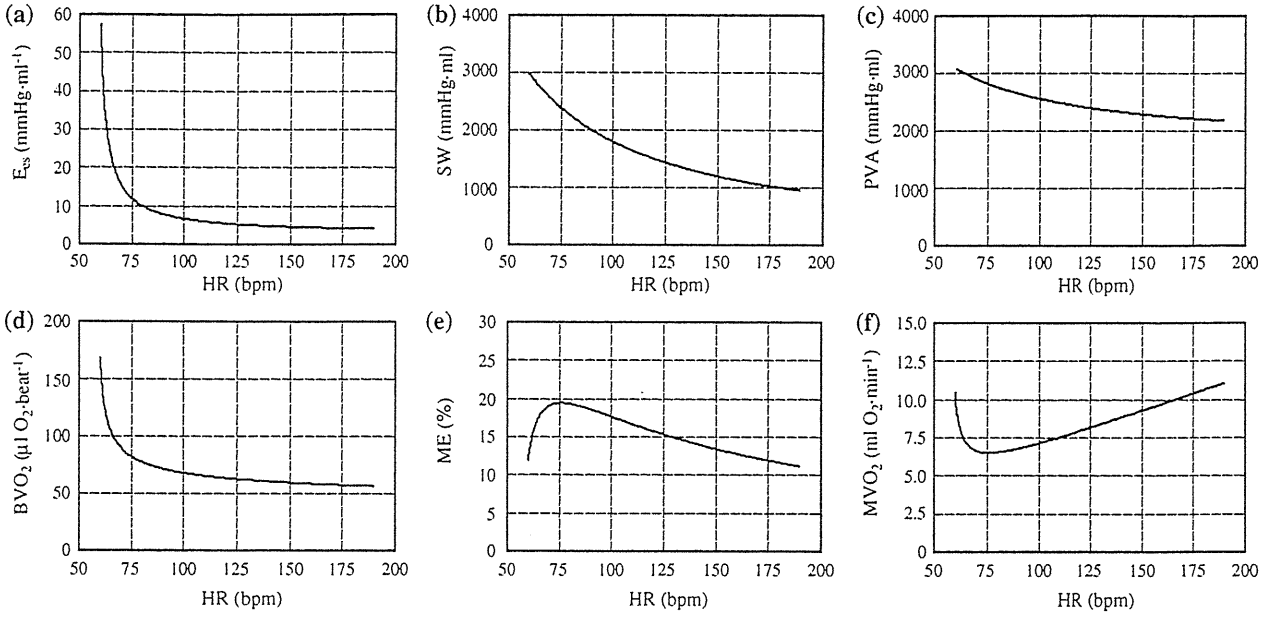

FIGURE 1. Simulated relations of heart rate (*HR*) with left ventricular end-systolic elastance (E_{es}) (a), left ventricular stroke work (*SW*) (b), left ventricular pressure–volume area (*PVA*) (c), left ventricular oxygen consumption per beat (BVO_2) (d), left ventricular mechanical efficiency (*ME*) (e), and left ventricular oxygen consumption per minute (MVO_2) (f), when systemic arterial pressure, cardiac output, and left atrial pressure are kept at fixed values. At *HR* of 75 bpm, *ME* becomes maximal (e), and MVO_2 becomes minimal (f).

previously.[30] *R* was calculated from the ratio of *AP* to *CO*. *ME* was calculated as the dimensionless ratio of *SW* to BVO_2.[19]

As indicated in Fig. 1, *HR* is inversely related to E_{es} (Fig. 1a), *SW* (Fig. 1b), *PVA* (Fig. 1c), and BVO_2 (Fig. 1d). Over the physiological range of *HR* for dogs (>80 bpm),[18] *ME* increases as *HR* is reduced (Fig. 1e) since *SW* increase is greater than BVO_2 increase; hence cardiac energetic efficiency is optimized. At *HR* of 75 bpm, *ME* becomes maximal and MVO_2 becomes minimal (Fig. 1f). When *HR* is reduced from 150 to 110 bpm, E_{es} increases from 4.6 to 5.9 mmHg mL^{-1} (29% increase) and *ME* increases from 13 to 17% (24% increase), whereas MVO_2 decreases from 8.9 to 7.2 mL O_2 min^{-1} (19% reduction). In addition to the simulation described above, we also simulated the relation of *HR* with MVO_2 for a variety of combinations of *AP* (80–120 mmHg), *CO* (80–100 mL min^{-1} kg^{-1}), and P_{LA} (10–20 mmHg). *HR* at which MVO_2 becomes minimal ranged from 50 to 75 bpm (data not shown). This indicates that as long as *HR* is within the physiological range, *HR* reduction together with compensatory increase of E_{es} consistently improves cardiac energetic efficiency and reduces MVO_2, irrespective of the target hemodynamics to be achieved.

Animal Preparation

After approval of the institutional Animal Care and Use Committee we studied 7 adult mongrel dogs (either sexes, 26 ± 4 kg). Anesthesia was induced with sodium pentobarbital (25 mg kg^{-1}). Animals were intubated endotracheally. Arterial pH, PO_2, and PCO_2 were maintained within the physiological ranges. Isoflurane (1.0%) was inhaled continuously during the experiment. After a median sternotomy and pericardial incision, an ultrasonic flow-meter (20A594, Transonics, Ithaca, NY) was placed around the ascending aorta to measure *CO*. Ultrasonic flow meters (2.5S273, Transonics, Ithaca, NY) were placed on the left circumflex and anterior descending coronary arteries to measure coronary blood flow. Fluid filled catheters were placed in the right femoral artery, left atrium and right atrium, and connected to pressure transducers (DX-200, Nihon Kohden, Tokyo, Japan) to measure *AP*, P_{LA}, and right atrial pressure, respectively. A catheter-tipped micromanometer (SPC-330A, Millar Instruments, Houston, TX) was introduced into the left ventricle to measure left ventricular pressure (LVP). A pair of pacing electrodes was fixed at the right atrial appendage for atrial pacing. A catheter (5F) was introduced into the coronary sinus via the right external jugular vein.

Two infusion pumps (CFV-3200, Nihon Kohden, Tokyo, Japan) for administering DOB and SNP, and a roller pump (Minipulse 3, Gilson, Middleton, WI) for administering DEX were attached to a catheter (5F) placed in the right femoral vein. These pumps were controlled with a laboratory computer (MA20V, NEC, Tokyo, Japan). From a catheter (5F) placed in the

right external jugular vein, FUR was injected following a command signal from the computer.

Analog signals of *AP*, *CO*, P_{LA}, right atrial pressure, LVP, and coronary blood flow were digitized (200 Hz, 12-bit) by the computer, and stored on a hard disk for off-line analysis. The digitized signals of *AP*, *CO*, and P_{LA} were smoothed by a low-pass filter with a time constant 10 s, and used as control variables for the regulator.

Automated Hemodynamic Regulator

Figure 2 is a schematic illustration of the automated hemodynamic regulator.[30] Once target values for *AP*, *CO*, and P_{LA} are defined and fed into the computer, it calculates the target values for S_L, *R*, and *V*. The subject's S_L, *R*, and *V* are calculated from the low-pass filtered *AP*, *CO*, and P_{LA} values. To minimize the differences between target and subject's S_L and *R*, proportional-integral feedback controllers adjust the infusion rates of DOB and SNP, respectively. To minimize the difference between target and subject's *V*, a nonlinear feedback controller adjusts the infusion of DEX or injection of FUR (see Appendix: Feedback control algorithms of the automatic hemodynamic regulator).

Experimental Protocols

After stabilization for 30 min, "baseline" hemodynamic data were recorded and blood samples were collected from the right femoral artery and the coronary sinus simultaneously for oxygen content determination (*Baseline*). Acute heart failure was induced by injecting glass microspheres (90 μm in diameter) to embolize the left circumflex coronary artery.[27] The amount of microspheres was adjusted to decrease *CO* to below 70 mL min^{-1} kg^{-1} or increase P_{LA} to above 15 mmHg. One hour after embolization, zatebradine (0.5 mg kg^{-1}) was administered intravenously to suppress the intrinsic atrial beat, and atrial pacing was then initiated to control *HR* at the level observed following coronary embolization. After the canine model of acute heart failure was established, hemodynamic measurements and blood sample collection were performed (*AHF*).

We activated the automated hemodynamic regulator with target values of 90–100 mmHg for *AP*, 80–100 mL kg^{-1} min^{-1} for *CO*, and 10–12 mmHg for P_{LA}. The regulator restored *AP*, *CO*, and P_{LA} to their respective target values within 30 min. After confirming stable hemodynamics, we collected blood samples as described above (*Initial HR*). We then reduced the pacing rate in steps of 10 or 20 bpm. The maximum *HR* reduction averaged 39 ± 12 bpm. For each *HR* step, we waited for hemodynamic stabilization, and then collected blood samples. After reaching the lowest HR (*Lowest HR*), we increased the *HR* stepwise back to the "Initial *HR*" to confirm the reproducibility of the hemodynamic control.

Data Analysis of LV Mechanoenergetics

We estimated E_{es} using a technique described previously.[14] In brief, the ratio of E_{es} to effective arterial elastance was estimated based on the fact that this ratio can be expressed as a function of P_{es}, LVP at which LV begins to eject, pre-ejection period, and

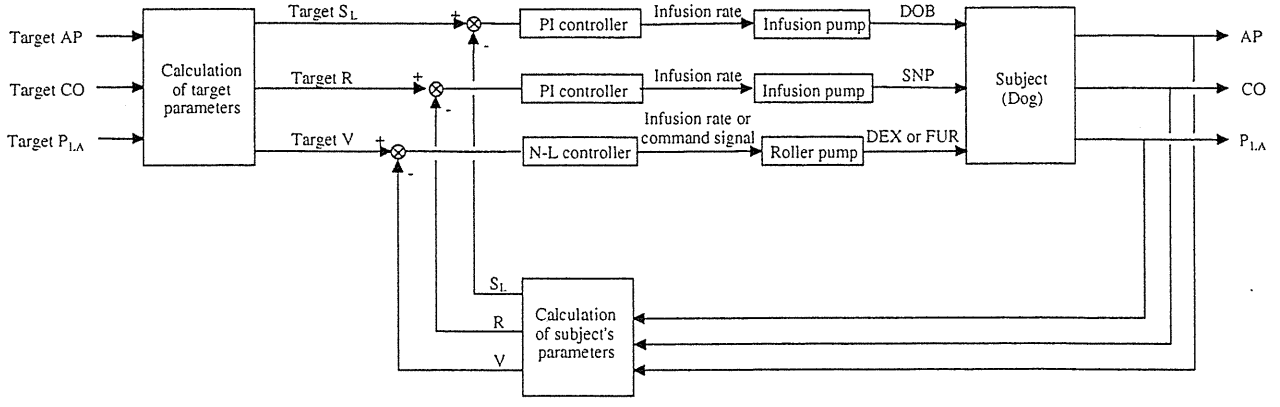

FIGURE 2. Schematic illustration of an automated hemodynamic regulator for simultaneous control of systemic arterial pressure (*AP*), cardiac output (*CO*), and left atrial pressure (P_{LA}). From target values of *AP*, *CO*, and P_{LA}, target values of functional slope of the left ventricular Starling's curve (S_L), systemic vascular resistance (*R*), and stressed blood volume (*V*) are determined. Subject's S_L, *V*, and *R* are calculated from low-pass filtered values of measured *AP*, *CO*, and P_{LA}. Proportional-integral (PI) feedback controllers adjust infusion rate of dobutamine (DOB) and sodium nitroprusside (SNP) to minimize the difference between target and subject's S_L and those of *R*, respectively. Nonlinear (N-L) feedback controller adjusts infusion of 10% dextran 40 (DEX) or injection of furosemide (FUR) to minimize the difference between target and subject's *V*.

ejection time. Effective arterial elastance is calculated as P_{es} divided by stroke volume. Therefore once we know the ratio, we can calculate E_{es}.[14] In this study, the end-diastolic point is defined as the moment when LV dP/dt exceeds 20% of positive dP/dt_{max}. The time point at which LV begins to eject is defined as the moment when the aortic flow begins. The end-systolic point is defined as the time when LV dP/dt decreases to 20% of LV dP/dt_{min}. Thus, pre-ejection period is obtained by subtracting the end-diastolic point from the time point at which LV begins to eject; and ejection time is obtained by subtracting the time point at which LV begins to eject from the end-systolic point.

SW was calculated using Eq. (3). *PVA* was calculated using Eq. (4). Oxygen contents of the blood samples were measured using a co-oxymeter (IL 682, Instrumentation Laboratory, Lexington, MA), and MVO_2 was calculated as the product of mean coronary blood flow and the coronary arteriovenous difference in oxygen content.[6] BVO_2 was calculated by dividing MVO_2 by *HR*. *ME* was calculated as described above.

Statistics

Group data are expressed as means ± SEM. Differences in hemodynamics, LV mechanoenergetics, and drug infusion rates among different conditions were evaluated using Student's paired *t*-test or a repeated-measures analysis of variance followed by Student-Newman–Keuls test. The level of statistical significance was defined as $p < 0.05$.

RESULTS

Hemodynamic and LV mechanoenergetic data at *Baseline* and *AHF* are summarized in Table 2. Coronary embolization nearly halved *CO* from 101 ± 5 to 62 ± 5 mL min^{-1} kg^{-1}, doubled P_{LA} from 8.9 ± 0.6 to 17.1 ± 0.7 mmHg, depressed E_{es} from 4.4 ± 0.7 to 2.5 ± 0.4 mmHg mL^{-1}, and halved MVO_2 from 5.8 ± 0.7 to 3.1 ± 0.2 mL min^{-1}. These changes are compatible with induction of acute ischemic heart failure.[27]

Figure 3 demonstrates the time courses of hemodynamics, the infusion rates of DOB and SNP, and the infused volume of DEX in a representative animal. Before activation of the regulator, *AP* was 108 mmHg, *CO* was 44 mL min^{-1} kg^{-1}, and P_{LA} was 16.9 mmHg. After activation of the regulator, the infusion rates of DOB, SNP, and DEX were adjusted automatically and S_L, *R*, and *V* reached their respective target values within 20 min. In this case, FUR was not used. By controlling S_L, *R*, and *V*, the regulator restored *AP*, *CO*, and P_{LA} to their respective target values (*AP*, 100 mmHg; *CO*, 80 mL min^{-1} kg^{-1}; P_{LA}, 10 mmHg). After attaining the target values at around 20 min, *AP*, *CO*, and P_{LA} were maintained at these levels stably throughout stepwise changes in *HR*. *HR* was reduced from 130 to 80 bpm in 10-bpm steps. Following *HR* reduction, the regulator increased the infusion rate of DOB to maintain S_L (Fig. 3). The regulator also decreased the infusion rate of SNP, and discontinued DEX infusion, thereby maintaining *R* and *V*, respectively. After attaining the lowest *HR* (80 bpm), *HR* was increased to 100 and 130 bpm. For each *HR* step, *AP*, *CO*, and P_{LA} were precisely controlled with minimum absolute errors from target values (error in *AP*, 3 ± 1 mmHg; error in CO, 1 ± 0 mL min^{-1} · kg^{-1}; error in P_{LA}, 0.3 ± 0.1 mmHg).

TABLE 2. Hemodynamic and left ventricular mechanoenergetic data at baseline (*Baseline*), and after coronary artery embolization (*AHF*).

	Baseline	*AHF*
HR, bpm	140 ± 7	146 ± 8
AP, mmHg	114 ± 4	97 ± 5†
CO, mL min^{-1} · kg^{-1}	101 ± 5	62 ± 5†
P_{LA}, mmHg	8.9 ± 0.6	17.1 ± 0.7†
E_{es}, mmHg mL^{-1}	4.4 ± 0.7	2.5 ± 0.4*
SW, mmHg mL	1667 ± 300	933 ± 91
PVA, mmHg mL	3292 ± 302	3235 ± 515
BVO_2, μL O_2 · $beat^{-1}$	41 ± 5	21 ± 1†
ME, %	36 ± 4	31 ± 4
MVO_2, mL O_2 · min^{-1}	5.8 ± 0.7	3.1 ± 0.2*

*$p < 0.05$, †$p < 0.01$ vs. *Baseline*. Values are mean ± SEM. *HR*, heart rate; *AP*, systemic arterial pressure; *CO*, cardiac output; P_{LA}, left atrial pressure; E_{es}, left ventricular (LV) end-systolic elastance; *SW*, LV stroke work; *PVA*, LV pressure–volume area; BVO_2, LV oxygen consumption per beat; *ME*, LV mechanical efficiency; MVO_2, LV oxygen consumption per minute.

Figure 4 demonstrates the relations of *HR* with E_{es} (Panel a), with *SW* (Panel b), with *PVA* (Panel c), with BVO_2 (Panel d), with *ME* (Panel e), and with MVO_2 (Panel f), which were determined at each *HR* step as shown in Fig. 3. E_{es} paralleled the infusion rate of DOB; the value increased from 2.9 to 5.3 mmHg mL^{-1} with *HR* reduction from 130 to 80 mmHg, and decreased to 3.3 mmHg mL^{-1} following the recovery of *HR* to 130 mmHg (Fig. 4a). *SW*, *PVA*, and BVO_2 increased with *HR* reduction, and decreased following the recovery of *HR* (Figs. 4b–d). Following *HR* reduction, since *SW* increased (+46%) to a greater extent than BVO_2 (+10%), *ME* increased from 51 to 67%. Following the recovery of *HR*, *ME* decreased to 52% (Fig. 4e). MVO_2 decreased from 3.3 to 2.3 mL O_2 min^{-1} with *HR* reduction, and increased to 3.0 mL O_2 min^{-1} following the recovery of *HR* (Fig. 4f). These changes in LV mechanoenergetic data are reasonably compatible with those predicted in *Theoretical analysis* (Fig. 1 compared with Fig. 4).

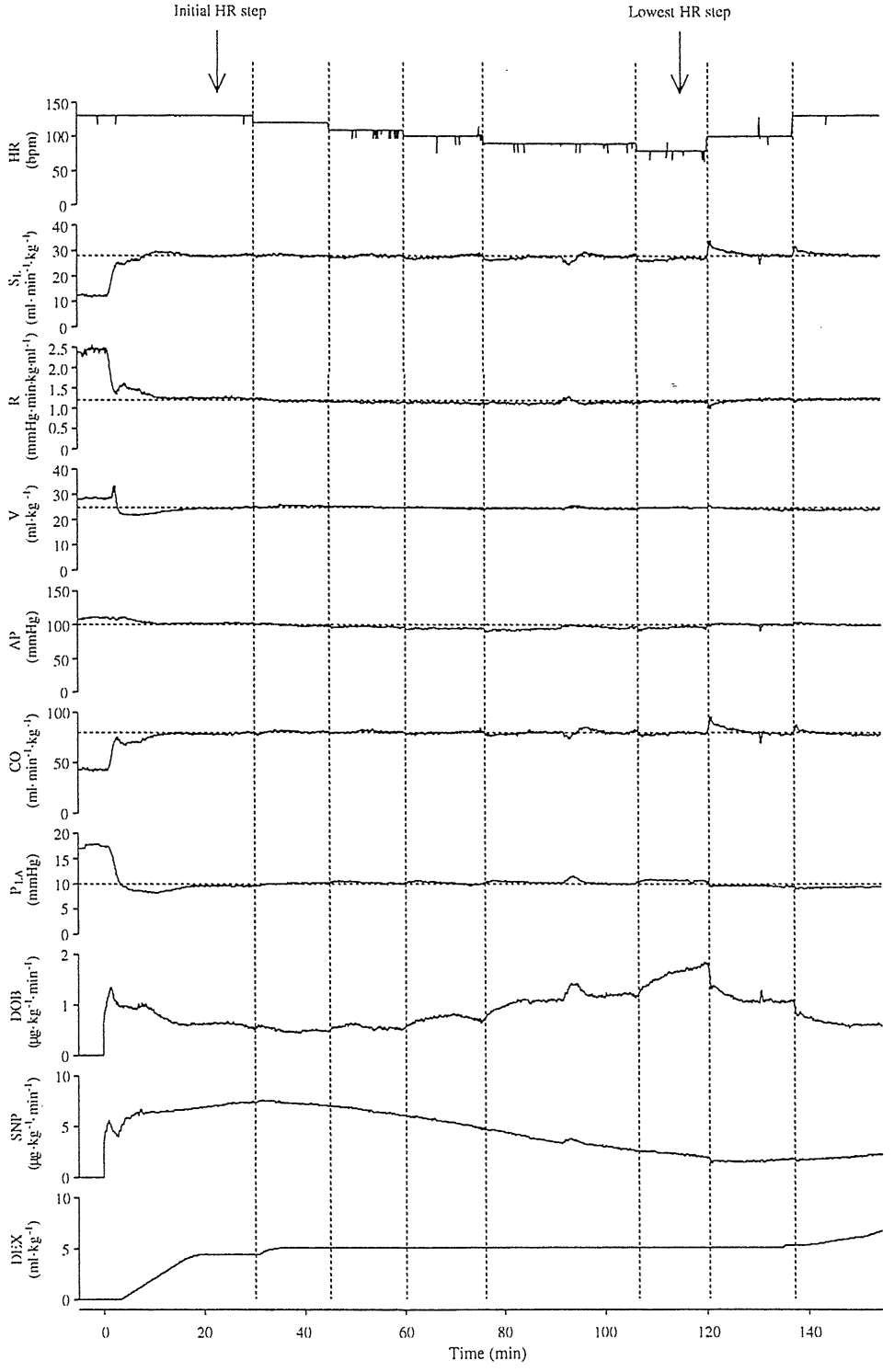

FIGURE 3. Time courses of heart rate (*HR*), S_L, *R*, *V*, *AP*, *CO*, P_{LA}, infusion rates of DOB, SNP, and accumulated volume of infused DEX in one representative animal during control of hemodynamics by the automated hemodynamic regulator. Target values of S_L, *R*, *V*, *AP*, *CO*, and P_{LA} are depicted by horizontal dotted lines in each trace. The *HR* steps (80–130 bpm) are separated by vertical dotted lines.

Table 3 summarizes the hemodynamic and drug infusion data at *AHF*, *Initial HR*, and *Lowest HR* in seven animals. In four animals, FUR (10 mg) was injected once between the *Initial HR* step and the *Lowest HR* step, and the total urine volume was 190–460 mL. Comparing the data at *Initial HR* and

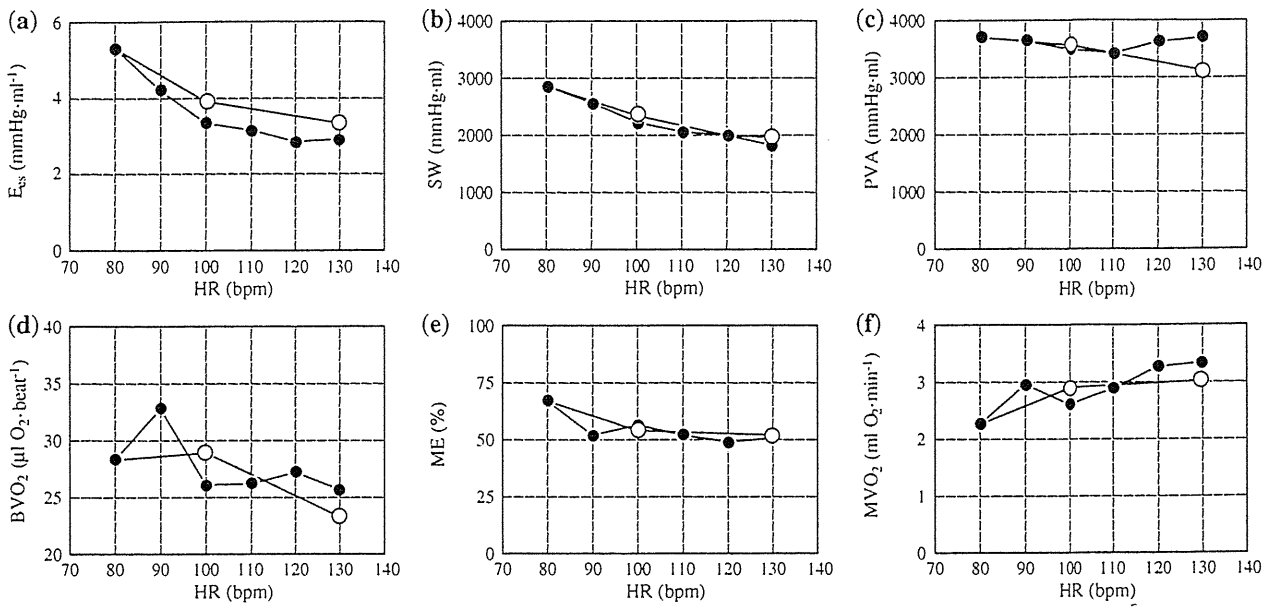

FIGURE 4. Relations of heart rate (*HR*) with left ventricular end-systolic elastance (E_{es}) (a), left ventricular stroke work (*SW*) (b), left ventricular pressure–volume area (*PVA*) (c), left ventricular oxygen consumption per beat (BVO_2) (d), left ventricular mechanical efficiency (*ME*) (e), and left ventricular oxygen consumption per minute (MVO_2) (f) determined at each *HR* step depicted in Fig. 3. •, measurement at each *HR* step while *HR* was reduced from 130 to 80 bpm; ○, measurement at each *HR* step when *HR* was increased from 100 to 130 bpm.

TABLE 3. Hemodynamic data and drug infusion rates after coronary artery embolization (*AHF*), at the initial *HR* (*Initial HR*), and at the lowest *HR* (*Lowest HR*).

	AHF	*Initial HR*	*Lowest HR*
HR, bpm	146 ± 8	146 ± 8	107 ± 7*,†
S_L, mL min^{-1} · kg^{-1}	18 ± 2	31 ± 1*	30 ± 1*
R, mmHg·min · kg · mL^{-1}	1.5 ± 0.2	1.0 ± 0.1*	1.0 ± 0.0*
V, mL · kg^{-1}	31 ± 1	27 ± 1*	27 ± 1*
DOB, μg min^{-1} kg^{-1}		1.4 ± 0.3	2.7 ± 0.5†
SNP, μg min^{-1} kg^{-1}		4.1 ± 0.8	2.4 ± 0.6
DEX, mL kg^{-1}		4.0 ± 0.7	0.8 ± 0.3†
AP, mmHg	97 ± 5	94 ± 3	93 ± 2
CO, mL min^{-1} kg^{-1}	62 ± 5	89 ± 3*	88 ± 3*
P_{LA}, mmHg	17.1 ± 0.7	10.5 ± 0.4*	10.9 ± 0.4*

*$p < 0.01$ vs. *AHF*, †$p < 0.01$ vs. *Initial HR*. Values are mean ± SEM. S_L, functional slope of the left ventricular Starling's curve; *R*, systemic vascular resistance; *V*, stressed blood volume; DOB, infusion rate of dobutamine; SNP, infusion rate of sodium nitroprusside; DEX, the value at *Initial HR* indicates the volume of dextran infused from the activation of the regulator until the *Initial HR*, the value at *Lowest HR* that from the *Initial HR* until the *Lowest HR*.

Lowest HR with those at *AHF*, S_L was increased while *R* and *V* were decreased significantly, indicating that cardiac function was improved while peripheral vasoconstriction and volume retention were relieved by our hemodynamic regulator. As a result, *CO* increased and P_{LA} decreased significantly. *AP*, *CO*, and P_{LA} were controlled precisely in all the animals with minimal absolute errors from target values (error in *AP*, 2 ± 0 mmHg; error in *CO*, 2 ± 0 mL min^{-1} kg^{-1}; error in P_{LA}, 0.4 ± 0.0 mmHg). Comparing the data at *Lowest HR* with those at *Initial HR*, HR decreased significantly (−27 ± 3%), the infusion rate of DOB increased significantly (+116 ± 23%), and the infused volume of DEX decreased significantly (−83 ± 7%).

Figure 5 summarizes the LV mechanoenergetic data at *AHF*, *Initial HR*, and *Lowest HR* in seven animals. When the data at *Initial HR* and *Lowest HR* were compared with those at *AHF*, E_{es}, *SW*, BVO_2, and *ME* increased, but *PVA* decreased significantly. MVO_2 at *Initial HR* also increased compared to that at *AHF*, although MVO_2 at *Lowest HR* was almost identical to that at *AHF*. The automated hemodynamic regulator restored normal hemodynamics with increased energy cost at *Initial HR*, but with diminished energy cost at *Lowest HR*. Comparing the data at *Lowest HR* with those at *Initial HR*, E_{es} increased significantly (+34 ± 14%), *SW* increased significantly (+37 ± 6%), and BVO_2 increased significantly (+12 ± 2%). Since *SW* increased to a greater extent than BVO_2, *ME* increased (+22 ± 6%) and MVO_2 decreased significantly (−17 ± 4%). Changes in the LV mechanoenergetic data following *HR* reduction averaged over seven animals are compatible with those predicted in *Theoretical analysis*.

DISCUSSION

To the best of our knowledge, we are the first to succeed in improving cardiac energetics without compromising normal hemodynamic conditions in acute

heart failure. Only by using our automated hemodynamic regulator, induced bradycardia improved cardiac energetic efficiency while restoring and strictly maintaining normal hemodynamic conditions in a canine model of acute heart failure.

Complicated Multiple Drug Infusions

Complicated regulations of multiple drug infusions were required to maintain *AP*, *CO*, and P_{LA} during *HR* reduction. It is difficult and unrealistic to control multiple drug infusions manually in hemodynamically unstable patients after bradycardia is induced.

Equation (1) indicates that *HR* reduction alone decreases S_L. In response to *HR* reduction, the negative feedback mechanism of our regulator automatically increases the infusion rate of DOB, which increases LV E_{es} and maintains S_L (Table 3, Fig. 5). An excessive increase in LV E_{es} can offset the MVO_2-decreasing effect of *HR* reduction. Therefore, the infusion rate of DOB must be precisely controlled. This is especially important when the oxygen cost of contractility is pathologically increased as observed in heart failure, where an oxygen-wasting effect of DOB may become crucial.[15]

DOB may increase *V*.[3] Our regulator effectively compensates the volume increasing effect of DOB by reducing or discontinuing DEX infusion, or by infusing FUR (Fig. 3, Table 3). DOB may also change *R*, and usually reduces *R*.[3] In some cases, the resistance-lowering effect of DOB is compensated by a decrease in infusion rate of SNP (Fig. 3). If these secondary effects of DOB are not adequately compensated, target hemodynamic conditions can no longer be maintained.

Comparison with Previous Hemodynamic Regulators

Apart from our automated hemodynamic regulator, several systems that automate the infusions of multiple cardiovascular drugs to control *AP* and *CO*, or *AP* and pulmonary arterial pressure have been reported.[17,23,33] However, it would be difficult to use these systems to improve the cardiac energetic efficiency. As indicated in *Theoretical analysis*, cardiac energetic efficiency is determined by *HR*, *AP*, *CO*, and P_{LA}. Those previous systems are incomplete for simultaneously control of all these multiple hemodynamic variables. Unstable performance of these systems sometimes results in drastic change of *HR*. Persistent oscillations of *CO* occurred following an abrupt increase in *HR* during automated hemodynamic control by a previously reported system.[23]

Our regulator controls the mechanical determinants of circulation, and as a result achieves target values for hemodynamic variables.[30] Previous systems[17,23,33]

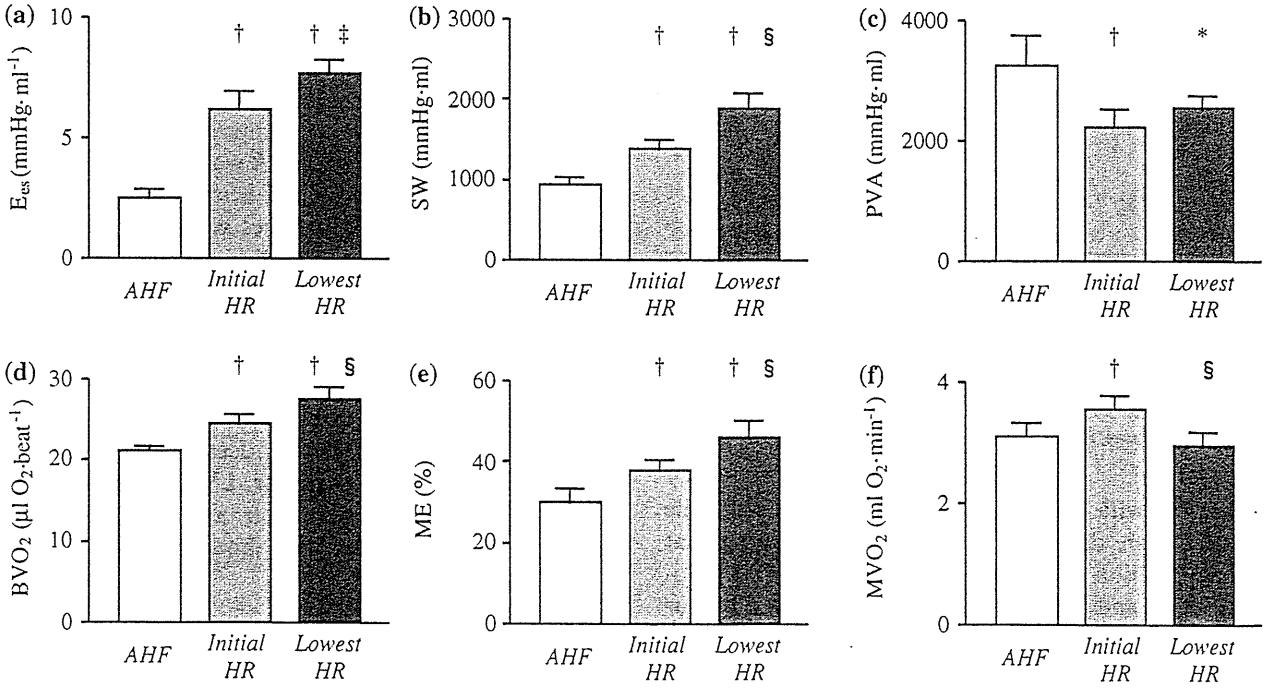

FIGURE 5. Left ventricular mechanoenergetic data after coronary artery embolization (*AHF*), at the initial *HR* (*Initial HR*), and at the lowest *HR* (*Lowest HR*). E_{es}, left ventricular (LV) end-systolic elastance; *SW*, LV stroke work; *PVA*, LV pressure–volume area; BVO_2, LV oxygen consumption per beat; *ME*, LV mechanical efficiency; MVO_2, LV oxygen consumption per minute. Data are means ± SEM. $^*p<0.05$, $^\dagger p<0.01$ vs. *AHF*. $^\ddagger p<0.05$, $^\S p<0.01$ vs. *Initial HR*.

attempted to control hemodynamic variables by estimating the apparent input–output relations between drug infusion and response of the controlled variables. In the systems that control *AP* and *CO*,[23,33] all possible input–output relations have to be estimated; namely, inotrope–*AP*, inotrope–*CO*, vasodilator–*AP*, and vasodilator–*CO* relations. The reason is that these drugs affect *AP* and *CO* simultaneously to almost the same degree. If this previous approach is applied to simultaneous control of *AP*, *CO*, and P_{LA}, at least 9 input–output relations have to be estimated, since at least 3 drugs are required to independently control the three variables. This would make the system extremely complicated, and therefore be practically unfeasible. The three drug controllers in our regulator (Fig. 2) are designed on the basis of only three input–output relations between drug infusion and response of the controlled parameter; namely, DOB–S_L, SNP–*R*, and DEX/FUR–*V*.[30] The fact that the three closed loops are effectively decoupled simplifies the entire system. This also permits a system operator, who would be a physician untrained in control engineering, to understand its behavior easily.

Comparison to Previous Studies on LV Mechanoenergetics

Several studies examined LV mechanoenergetics under LV inotropy and bradycardia *in vivo*.[16,25] Single drug or two-drug combinations were used and infusions were titrated manually. However, *HR* reduction inevitably induced changes in *AP*, *CO*, or P_{LA} in these studies.

Shen *et al.*[25] compared the inotropic/chronotropic effects and MVO_2 in response to the sodium channel enhancer LY341311 with those in response to dobutamine in dogs with heart failure. LY341311 increased LV dP/dt_{max} and decreased *HR*. At similar levels of inotropic response and similar levels of *AP* and P_{LA}, dobutamine increased MVO_2 whereas LY341311 did not. These results suggested a favorable effect of LY341311 on myocardial energetics. However, the investigators did not evaluate *CO*. Since left ventricular end-diastolic volume and ventricular fractional shortening were also comparable between the two groups, *CO* must be lower in the LY341311 group in proportion to the magnitude of HR reduction. The favorable effect of LY341311 on myocardial energetics might be in part at the sacrifice of *CO*, i.e., at the sacrifice of peripheral perfusion.

Absolute values of *ME* obtained in the present study (30–70%) were higher than those reported in previous studies (<30%).[19,26,28] Differences in experimental methods may be one reason for this discrepancy. We measured the coronary blood flow using the ultrasonic flow meters placed on the anterior descending and circumflex coronary arteries. However, owing to technical difficulties, blood flow in most proximal branches of the anterior descending artery, such as the first septal and/or first diagonal branches were not included. On the other hand, previous studies using coronary sinus thermo-dilution catheters[19,26] or cross-circulated dog heart preparations[28] were able to measure total coronary artery blood flow including that in proximal branches. Systematic underestimation of coronary blood flow in our study might result in systematic underestimation of ventricular oxygen consumption, and as a result overestimation of *ME*. In addition, *SW* calculated by Eq. (3) does not fully describe the net external work done by LV per cardiac cycle, since diastolic work performed on the ventricle was assessed inaccurately.[11] However, *SW* calculated by Eq. (3) and the net external work determined by the LV pressure–volume loop correlates with high linearity.[11] Taken together, it is fair to say that the direction and magnitude of changes in MVO_2 and *ME* were evaluated accurately in the present study.

Comparison with Beta-blockade Alone

The degree of reduction in MVO_2 (17%, *Lowest HR* vs. *Initial HR* in Fig. 5f) when HR was reduced by 30% in the present experiment is less than that observed in beta-blockade treatment. For example, atenolol decreased MVO_2 by 40% when *HR* was reduced by 30% in dogs during exercise.[6] Negative ventricular inotropy accompanying *HR* reduction accounts for the further reduction in MVO_2 achieved by beta-blockade.[6] However, in acute heart failure, use of beta-blockers is contraindicated owing to its adverse effects on systemic hemodynamics.[1,5] Taken together, the degree of reduction in MVO_2 obtained in this study is reasonable considering that it is achieved without sacrificing the normal hemodynamic condition.

Use of Specific Bradycardic Agent

Under physiological conditions, HR and the ventricular contractility are internally coupled, and is known as the force frequency relationship.[8] In the present study, co-administration of zatebradine with DOB uncoupled this relationship and allowed us to change *HR* and the ventricular contractility (E_{es}) in opposite directions (Fig. 4a).[24] Zatebradine selectively inhibits funny current, which is a primary sinoatrial node pacemaker current, and does not inhibit calcium channel.[12] Therefore, zatebradine reduced *HR* with little influence on the positive inotropic effect of DOB.

Zatebradine has not been further developed for clinical use. Its successor ivabradine belongs to the

same class of selective *HR*-lowering agents that act specifically on the sinoatrial node, and has been approved for clinical application.[4] The fact that ivabradine reduces *HR* dose dependently suggests that in future clinical application of our regulator, we may be able to control the *HR* reduction by titrating ivabradine infusion only without the need of atrial pacing.

Limitations

Figure 1 suggests that if heart rate is reduced beyond a critical value at which MVO_2 becomes minimal, cardiac energetics does not improve, or even deteriorates. This finding indicates that over-reduction of *HR* below the critical value should be avoided when applying the present framework to hemodynamic management. As indicated in Theoretical analysis, satisfactory management would be generally achieved in dogs if *HR* is maintained above 75 bpm. For clinical application of the present framework, a method has to be established to estimate the critical *HR* in each cardiac patient.

We directly measured *CO* and P_{LA} in open chest condition, which is not relevant to the clinical setting. Several methods have been developed to continuously monitor these variables in closed chest conditions.[2] Integrating these methods into our regulator would bring the clinical application of our regulator closer to reality.

The neurohormonal-mediated reflexes, which might have been attenuated by anesthesia in the present study, may cause unstable automated hemodynamic control under conscious condition. Patients with acute heart failure usually have a long history of cardiovascular dysfunction resulting from extensive myocardial remodeling, down-regulation of major receptors controlling HR, contractility, and myocardial oxygen metabolism.[22] This was not the case in our model as the dogs were treated with glass microspheres to induce acute heart failure. Response to our interventional strategy in a chronic heart failure model may be different from that observed in this study. Further studies on these respects are clearly required.

Although reduction in MVO_2 following HR reduction was statistically significant, the degree of reduction was rather mild (Fig. 5f). Furthermore, increase in ventricular contractility suggests that calcium transient may be increased on a single beat basis. Calcium overload closely correlates with myocardial damage and cell death.[21] Whether the improvement in myocardial energetics as achieved in the present study really ameliorates the myocardial damage in acute heart failure remains to be evaluated in future studies.

CONCLUSION

In a canine acute heart failure model, direct control of the mechanical determinants of circulation using an automated hemodynamic regulator improved cardiac energetic efficiency while restoring normal hemodynamic conditions. Our system may be a useful tool in managing hemodynamically unstable patients with acute heart failure.

APPENDIX

Feedback Control Algorithms of the Automatic Hemodynamic Regulator

To minimize the difference between target and subject's S_L (ΔS_L = target S_L—subject's S_L) and those of R (ΔR = target R—subject's R), the proportional-integral (PI) feedback controllers adjust the infusion rates of DOB and SNP, respectively (Fig. 2). In the PI controller (Fig. 6), ΔS_L (or ΔR) and the difference integrated with an integral gain (K_i) are summed and scaled by a proportional gain (K_p) to give the infusion rate of DOB (or SNP). PI gain constants for DOB infusion [$K_i = 0.01\ s^{-1}$, $K_p = 0.06\ \mu g\ kg^{-1}\ min^{-1}$ ($mL\ min^{-1}\ kg^{-1})^{-1}$] and for SNP infusion [$K_i = 0.007\ s^{-1}$, $K_p = -1.37\ \mu g\ kg^{-1}\ min^{-1}$ (mmHg min $ml^{-1}\ kg)^{-1}$] were determined on the basis of open-loop response of S_L and R to the infusion of DOB and SNP, respectively.[30]

To minimize the difference between target and subject's V (ΔV = target V—subject's V), a nonlinear (N-L) feedback controller (Fig. 2) adjusts the infusion of DEX or injection of FUR based on the following "if-then" rules:

Rule 1: If $\Delta V \geq 1\ mL\ kg^{-1}$ then infuse DEX at $10\ mL\ min^{-1}$

Rule 2: If $\Delta V \leq -2\ mL\ kg^{-1}$ then inject FUR (10 mg) at 10 min intervals

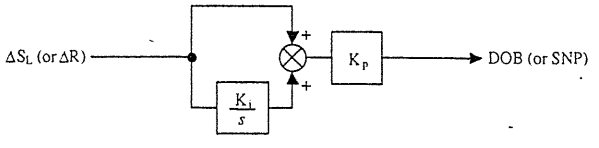

FIGURE 6. Block diagram of the PI controller in the automated hemodynamic regulator. ΔS_L and ΔR denote the difference between target and subject's S_L, and between target and subject's R, respectively. K_I and K_p represent the integral and proportional gain constants, respectively. s is a Laplace operator.

The "if-then" rules were determined on the basis of the open-loop response of V to the infusion of DEX and FUR.[30]

ACKNOWLEDGMENT

This study was supported by Grant-in-Aid for Scientific Research (C) (18500358, 20500404) from the Ministry of Education, Culture, Sports, Science and Technology, by a research grant from Nakatani Foundation of Electronic Measuring Technology Advancement, and by Health and Labour Sciences Research Grants (H19-nano-ippan-009) from the Ministry of Health, Labour and Welfare of Japan.

REFERENCES

[1]Antman, E. M., D. T. Anbe, P. W. Armstrong, E. R. Bates, L. A. Green, M. Hand, J. S. Hochman, H. M. Krumholz, F. G. Kushner, G. A. Lamas, C. J. Mullany, J. P. Ornato, D. L. Pearle, M. A. Sloan, S. C. Smith, Jr., J. S. Alpert, J. L. Anderson, D. P. Faxon, V. Fuster, R. J. Gibbons, G. Gregoratos, J. L. Halperin, L. F. Hiratzka, S. A. Hunt, A. K. Jacobs, and J. P. Ornato. American College of Cardiology; American Heart Association; Canadian Cardiovascular Society ACC/AHA guidelines for the management of patients with ST-elevation myocardial infarction–executive summary. A report of the American College of Cardiology/American Heart Association Task Force on Practice Guidelines (Writing Committee to revise the 1999 guidelines for the management of patients with acute myocardial infarction). *J. Am. Coll. Cardiol.* 44:671–719, 2004. doi:10.1016/j.jacc.2004.07.002.

[2]Bein, B., F. Worthmann, P. H. Tonner, A. Paris, M. Steinfath, and J. Hedderich. Comparison of esophageal Doppler, pulse contour analysis, and real-time pulmonary artery thermodilution for the continuous measurement of cardiac output. *J. Cardiothorac. Vasc. Anesth.* 18:185–189, 2004. doi:10.1053/j.jvca.2004.01.025.

[3]Binkley, P. F., K. D. Murray, K. M. Watson, P. D. Myerowitz, and C. V. Leier. Dobutamine increases cardiac output of the total artificial heart. Implications for vascular contribution of inotropic agents to augmented ventricular function. *Circulation* 84:1210–1215, 1991.

[4]Borer, J. S., K. Fox, P. Jaillon, and G. Lerebours. Antianginal and antiischemic effects of ivabradine, an I(f) inhibitor, in stable angina: a randomized, double-blind, multicentered, placebo-controlled trial. *Circulation* 107: 817–823, 2003. doi:10.1161/01.CIR.0000048143.25023.87.

[5]Choong, C. Y., G. S. Roubin, P. J. Harris, Y. Tokuyasu, W. F. Shen, G. J. Bautovich, and D. T. Kelly. A comparison of the effects of beta-blockers with and without intrinsic sympathomimetic activity on hemodynamics and left ventricular function at rest and during exercise in patients with coronary artery disease. *J. Cardiovasc. Pharmacol.* 8:441–448, 1986. doi:10.1097/00005344-198605000-00001.

[6]Colin, P., B. Ghaleh, X. Monnet, J. Su, L. Hittinger, J. F. Giudicelli, and A. Berdeaux. Contributions of heart rate and contractility to myocardial oxygen balance during exercise. *Am. J. Physiol. Heart Circ. Physiol.* 284:H676–H682, 2003.

[7]Colucci, W. S. Myocardial and vascular actions of milrinone. *Eur. Heart J.* 10(Suppl C):32–38, 1989.

[8]Freeman, G. L., W. C. Little, and R. A. O'Rourke. Influence of heart rate on left ventricular performance in conscious dogs. *Circ. Res.* 61:455–464, 1987.

[9]Gingrich, K. J., and R. J. Roy. Modeling the hemodynamic response to dopamine in acute heart failure. *IEEE Trans. Biomed. Eng.* 38:267–272, 1991. doi:10.1109/10.133208.

[10]Glantz, S. A. Ventricular pressure–volume curve indices change with end-diastolic pressure. *Circ. Res.* 39:772–778, 1976.

[11]Glower, D. D., J. A. Spratt, N. D. Snow, J. S. Kabas, J. W. Davis, C. O. Olsen, G. S. Tyson, D. C. Sabiston, Jr., and J. S. Rankin. Linearity of the Frank–Starling relationship in the intact heart: the concept of preload recruitable stroke work. *Circulation* 71:994–1009, 1985.

[12]Guth, B. D., and T. Dietze. If current mediates β-adrenergic enhancement of heart rate but not contractility in vivo. *Basic Res. Cardiol.* 90:192–202, 1995. doi:10.1007/BF00805662.

[13]Hamlin, R. L., T. Nakayama, H. Nakayama, and C. A. Carnes. Effects of changing heart rate on electrophysiological and hemodynamic function in the dog. *Life Sci.* 72:1919–1930, 2003. doi:10.1016/S0024-3205(03)00015-8.

[14]Hayashi, K., K. Shigemi, T. Shishido, M. Sugimachi, and K. Sunagawa. Single-beat estimation of ventricular end-systolic elastance-effective arterial elastance as an index of ventricular mechanoenergetic performance. *Anesthesiology* 92:1769–1776, 2000. doi:10.1097/00000542-200006000-00037.

[15]Hayashi, Y., M. Takeuchi, H. Takaoka, K. Hata, M. Mori, and M. Yokoyama. Alteration in energetics in patients with left ventricular dysfunction after myocardial infarction: increased oxygen cost of contractility. *Circulation* 93:932–939, 1996.

[16]Hettrick, D. A., P. S. Pagel, D. Lowe, J. P. Tessmer, and D. C. Warltier. Increases in inotropic state without change in heart rate: combined use of dobutamine and zatebradine in conscious dogs. *Eur. J. Pharmacol.* 316:237–244, 1996. doi:10.1016/S0014-2999(96)00688-7.

[17]Hoeksel, S. A., J. A. Blom, J. R. Jansen, J. G. Maessen, and J. J. Schreuder. Automated infusion of vasoactive and inotropic drugs to control arterial and pulmonary pressures during cardiac surgery. *Crit. Care Med.* 27:2792–2798, 1999. doi:10.1097/00003246-199912000-00031.

[18]Iellamo, F., J. A. Sala-Mercado, M. Ichinose, R. L. Hammond, M. Pallante, T. Ichinose, L. W. Stephenson, and D. S. O'Leary. Spontaneous baroreflex control of heart rate during exercise and muscle metaboreflex activation in heart failure. *Am. J. Physiol. Heart Circ. Physiol.* 293:H1929–H1936, 2007. doi:10.1152/ajpheart.00564.2007.

[19]Kim, I. S., H. Izawa, T. Sobue, H. Ishihara, F. Somura, T. Nishizawa, K. Nagata, M. Iwase, and M. Yokota. Prognostic value of mechanical efficiency in ambulatory patients with idiopathic dilated cardiomyopathy in sinus rhythm. *J. Am. Coll. Cardiol.* 39:1264–1268, 2002. doi:10.1016/S0735-1097(02)01775-8.

[20]Knaapen, P., T. Germans, J. Knuuti, W. J. Paulus, P. A. Dijkmans, C. P. Allaart, A. A. Lammertsma, and

F. C. Visser. Myocardial energetics and efficiency: current status of the noninvasive approach. *Circulation* 115:918–927, 2007. doi:10.1161/CIRCULATIONAHA.106.660639.

[21]Miyata, H., E. G. Lakatta, M. D. Stern, and H. S. Silverman. Relation of mitochondrial and cytosolic free calcium to cardiac myocyte recovery after exposure to anoxia. *Circ. Res.* 71:605–613, 1992.

[22]Nikolaidis, L. A., T. Hentosz, A. Doverspike, R. Huerbin, C. Stolarski, Y. T. Shen, and R. P. Shannon. Catecholamine stimulation is associated with impaired myocardial O_2 utilization in heart failure. *Cardiovasc. Res.* 53:392–404, 2002. doi:10.1016/S0008-6363(01)00490-4.

[23]Rao, R. R., B. Aufderheide, and B. W. Bequette. Experimental studies on multiple-model predictive control for automated regulation of hemodynamic variables. *IEEE Trans. Biomed. Eng.* 50:277–288, 2003. doi:10.1109/TBME.2003.808813.

[24]Schipke, J. D., Y. Harasawa, S. Sugiura, J. Alexander, Jr., and D. Burkhoff. Effect of a bradycardic agent on the isolated blood-perfused canine heart. *Cardiovasc. Drugs Ther.* 5:481–488, 1991.

[25]Shen, W., R. M. Gill, B. D. Jones, J. P. Zhang, A. K. Corbly, and M. I. Steinberg. Combined inotropic and bradycardic effects of a sodium channel enhancer in conscious dogs with heart failure: a mechanism for improved myocardial efficiency compared with dobutamine. *J. Pharmacol. Exp. Ther.* 303:673–680, 2002. doi:10.1124/jpet.303.2.673.

[26]Shinke, T., M. Takeuchi, H. Takaoka, and M. Yokoyama. Beneficial effects of heart rate reduction on cardiac mechanics and energetics in patients with left ventricular dysfunction. *Jpn. Circ. J.* 63:957–964, 1999. doi:10.1253/jcj.63.957.

[27]Smiseth, O. A., and O. D. Mjos. A reproducible and stable model of acute ischaemic left ventricular failure in dogs. *Clin. Physiol.* 2:225–239, 1982. doi:10.1111/j.1475-097X.1982.tb00027.x.

[28]Suga, H. Ventricular energetics. *Physiol. Rev.* 70:247–277, 1990.

[29]Suga, H, Y. Yasumura, T. Nozawa, S. Futaki, Y. Igarashi, and Y. Goto. Prospective prediction of O_2 consumption from pressure–volume area in dog hearts. *Am. J. Physiol.* 252:H1258–H1264, 1987.

[30]Uemura, K., A. Kamiya, I. Hidaka, T. Kawada, S. Shimizu, T. Shishido, M. Yoshizawa, M. Sugimachi, and K. Sunagawa. Automated drug delivery system to control systemic arterial pressure, cardiac output, and left heart filling pressure in acute decompensated heart failure. *J. Appl. Physiol.* 100:1278–1286, 2006. doi:10.1152/japplphysiol.01206.2005.

[31]Uemura, K., T. Kawada, A. Kamiya, T. Aiba, I. Hidaka, K. Sunagawa, and M. Sugimachi. Prediction of circulatory equilibrium in response to changes in stressed blood volume. *Am. J. Physiol. Heart Circ. Physiol.* 289:H301–H307, 2005. doi:10.1152/ajpheart.01237.2004.

[32]Uemura, K., M. Sugimachi, T. Kawada, A. Kamiya, Y. Jin, K. Kashihara, and K. Sunagawa. A novel framework of circulatory equilibrium. *Am. J. Physiol. Heart Circ. Physiol.* 286:H2376–H2385, 2004. doi:10.1152/ajpheart.00654.2003.

[33]Yu, C., R. J. Roy, H. Kaufman, and B. W. Bequette. Multiple-model adaptive predictive control of mean arterial pressure and cardiac output. *IEEE Trans. Biomed. Eng.* 39:765–778, 1992. doi:10.1109/10.148385.

Annals of Biomedical Engineering, Vol. 37, No. 1, January 2009 (© 2008) pp. 112–128
DOI: 10.1007/s10439-008-9599-4

Wavelet-Based System Identification of Short-Term Dynamic Characteristics of Arterial Baroreflex

KOJI KASHIHARA,[1,2] TORU KAWADA,[3] MASARU SUGIMACHI,[3] and KENJI SUNAGAWA[4]

[1]Hypertension and Stroke Research Laboratory, Royal North Shore Hospital, University of Sydney, Ground Floor, Building 10, Royal North Shore Hospital, St. Leonards, NSW 2065, Australia; [2]National Institute for Longevity Sciences, NCGG, 36-3 Gengo, Morioka-machi, Obu City, Aichi 474-8511, Japan; [3]Department of Cardiovascular Dynamics, National Cardiovascular Center Research Institute, 5-7-1 Fujishirodai, Suita, Osaka 565-8565, Japan; and [4]Department of Cardiovascular Medicine, Kyushu University, 3-1-1, Maidashi, Higashi-ku, Fukuoka 812-8582, Japan

(Received 1 February 2008; accepted 31 October 2008; published online 12 November 2008)

Abstract—The assessment of arterial baroreflex function in cardiovascular diseases requires quantitative evaluation of dynamic and static baroreflex properties because of the frequent modulation of baroreflex properties with unstable hemodynamics. The purpose of this study was to identify the dynamic baroreflex properties from transient changes of step pressure inputs with background noise during a short-duration baroreflex test in anesthetized rabbits with isolated carotid sinuses, using a modified wavelet-based time-frequency analysis. The proposed analysis was able to identify the transfer function of baroreflex as well as static properties from the transient input-output responses under normal [gain at 0.04 Hz from carotid sinus pressure (CSP) to arterial pressure ($n = 8$); 0.29 ± 0.05 at low (40–60 mmHg), 1.28 ± 0.12 at middle (80–100 mmHg), and 0.38 ± 0.07 at high (120–140 mmHg) CSP changes] and pathophysiological [gain in control vs. phenylbiguanide ($n = 8$); 0.32 ± 0.07 vs. 0.39 ± 0.09 at low, 1.39 ± 0.15 vs. 0.59 ± 0.09 ($p < 0.01$) at middle, and 0.35 ± 0.04 vs. 0.15 ± 0.02 ($p < 0.01$) at high CSP changes] conditions. Subsequently, we tested the proposed wavelet-based method under closed-loop baroreflex responses; the simulation study indicates that it may be applicable to clinical situations for accurate assessment of dynamic baroreflex function. In conclusion, the dynamic baroreflex property to various pressure inputs could be simultaneously extracted from the step responses with background noise.

Keywords—Baroreceptor reflex, Sympathetic nerve activity, Arterial pressure, Transfer function, Dynamic characteristics.

INTRODUCTION

Arterial baroreflex is a crucial negative feedback system because of the quick stabilization of arterial pressure (AP) against external pressure disturbances.[12,30] The assessment of arterial baroreflex function would require quantifying the dynamic as well as static properties[15,46] because the baroreflex gain or sensitivity is frequently modulated during cardiovascular diseases.[6,36,39] Because quick responses of autonomic nerves and AP mainly through the brainstem[3] might contain the unknown characteristics changing by the minute in acute cardiovascular diseases,[25] the short-term dynamic system identification might relate to the novel finding under such nonstationary condition. Laboratory and spontaneous baroreflex methods[37] are widely used in human and animal studies. The laboratory method requires invasive pharmacological or mechanical pressure interventions, and it may be suitable for estimation of the mechanism of AP regulation through the sympathetic as well as vagal baroreflex.[7,45] The spontaneous baroreflex method aims to assess cardiovagal activity noninvasively using systolic AP and heart rate variability.[5] These methods have various merits under the baroreflex testing conditions, but remain debatable because of complicated mechanisms.[27,37,40,43]

In the laboratory method, the standard analysis of sympathetic baroreflex has been performed mainly in the time[10,16] or frequency domain.[1,29,35,44] The time-domain analysis has evaluated the stable or maximal gain around the operating point, but may not characterize the impaired dynamic baroreflex properties accurately in cardiovascular patients with unstable hemodynamics and background noise. In the frequency domain, fast Fourier transform (FFT) analysis[31] has identified dynamic baroreflex properties under such noisy condition, but requires longer data segments to cancel the background noise and to identify the dynamic properties with low-frequency band,[38] indicating difficulties to extract short-term changes. In

Address correspondence to Koji Kashihara, Hypertension and Stroke Research Laboratory, Royal North Shore Hospital, University of Sydney, Ground Floor, Building 10, Royal North Shore Hospital, St. Leonards, NSW 2065, Australia. Electronic mail: kojikasi-nils@umin.ac.jp

the spontaneous baroreflex method, the analytical time window based on short-time FFT[5] (STFFT) has been adjusted to evaluate the time-varying gain around the operating point. However, this method may not be suitable for the evaluation of short-term changes in baroreflex properties for AP regulation through sympathetic as well as vagal nerves, at multiple pressure points with background noise. A combination of time and frequency analysis using wavelet transform may be able to identify the dynamic baroreflex properties efficiently regardless of background noise[2,4] by virtue of its high temporal resolution.[34] If dynamic and static characteristics in cardiovascular patients with unstable hemodynamics can be identified in a short-duration baroreflex test, various pathophysiological characteristics may be gained simultaneously.

The first purpose of this study was to examine whether a proposed wavelet-based time-frequency analysis was able to identify the dynamic as well as static baroreflex properties in animals from transient step pressure inputs with background noise during a short-duration test. Next, the proposed analysis was applied to identify unknown dynamic baroreflex properties in nonlinear AP input ranges during the Bezold-Jarisch reflex (BJR). We hypothesized that the proposed analysis could evaluate the baroreflex transfer properties from a short-term protocol, simultaneously at various pressure inputs under normal and BJR conditions. Finally, we examined the possibility of applying the new analysis to human studies to evaluate the dynamic baroreflex for AP regulation through the sympathovagal activity.

METHODS

Pathways of Baroreflex Functions

Under the carotid sinus open-loop condition, we defined the total loop as the system from carotid sinus pressure (CSP) input to AP output, which is divided into the neural arc as the subsystem from CSP input to renal sympathetic nerve activities (RSNA) output and the peripheral arc as the subsystem from RSNA input to AP output.[15] The cardiac baroreflex was defined as the system from CSP to heart rate (HR) response,[52] which may represent sympathovagal control of the heart through the baroreflex.

Surgical Preparations

Animals were cared for in accordance with the *Guiding Principles for the Care and Use of Animals in the Field of Physiological Sciences* approved by the Physiological Society of Japan. Japanese white rabbits were anesthetized with an intravenous injection (2 mL/kg) of a mixture of urethane (250 mg/mL) and α-chloralose (40 mg/mL) followed by a continuous administration (0.2–0.3 mL/kg/h, i.v.). The rabbits were artificially ventilated with oxygen-enriched room air at 0.6 Hz. Raw wave of AP was measured from the right femoral artery, using a high-fidelity pressure transducer (Millar Instruments, Houston, TX). A double-lumen catheter was placed into the right femoral vein for drug administration. The aortic depressor nerves identified by arterial pulse-synchronous activities were sectioned, while bilateral vagi were kept intact. Bilateral carotid sinuses were isolated from the systemic circulation by ligating the external and internal carotid arteries, and were filled with warm physiological saline through catheters inserted into the common carotid arteries. CSP was adjusted with a servo-controlled piston pump controlled by a computer system.

The left renal sympathetic nerve was exposed and a pair of stainless steel wire electrodes (Bioflex wire AS633, Cooner Wire) was attached. The nerve fibers distal to the electrodes were crushed by tight ligature to eliminate afferent signals from the kidney, and were covered in silicone gel (Semicosil 932A/B, Wacker Silicones). The preamplified nerve signal, band-pass filtered at 150–1000 Hz, was full-wave rectified and low-pass filtered at a cutoff frequency of 30 Hz (i.e. Op-amp RC integrator) to quantify nerve activity. Pancuronium bromide (0.3 mg/kg, i.v.) was administered to prevent muscular activity. The body temperature was kept at 38 °C.

Step Input Protocol

The carotid sinus baroreflex negative feedback loop was closed by adjusting CSP to AP level for 20 min after the surgical preparations (8 rabbits weighing 2.7–3.0 kg). The feedback loop was then opened and CSP was maintained at 40 mmHg for 4 min until the AP response reached a steady state. CSP was then increased from 40 to 160 mmHg in increments of 20 mmHg every minute (CSP_{40-60}, CSP_{60-80}, CSP_{80-100}, $CSP_{100-120}$, $CSP_{120-140}$, and $CSP_{140-160}$ changes). The single trial was repeated three times every rabbit. Data were sampled at 200 Hz and were averaged every 40 points for analysis (i.e. pulsatile AP signals were averaged every 0.2 s). HR (beats/min) was counted from the pulse waves of raw AP signals, which are well known as waves synchronized with ECG.[33] RSNA data of each animal were presented in arbitrary units (a.u.), with 1-min averaged background noise taken as zero level and 10-s averaged RSNA at CSP of 40 mmHg in normal condition set as unity.

Data Analysis

Identification of Dynamic Baroreflex

After the recorded data (three times) of CSP, RSNA, AP and HR were averaged in each animal, the signals were convoluted by complex Morlet wavelet, $w(t, f_0)$:[48,49]

$$w(t, f_0) = \frac{1}{\sqrt{\sigma_t\sqrt{\pi}}} \cdot \exp\left(\frac{-t^2}{2\sigma_t^2}\right) \cdot \exp(2\pi f_0 it) \qquad (1)$$

where the $(\sigma_t\sqrt{\pi})^{-1/2}$ normalizes the wavelets to be unity total energy, and the $\exp(-t^2/2\sigma_t^2)$ is a Gaussian shape with the central frequency f_0 at time t. The standard deviation (σ_t) of the time domain is inversely proportional to the standard deviation (σ_f) of the frequency domain [$\sigma_f = (2\pi\sigma_t)^{-1}$]. A constant ratio, f_0/σ_f, determines the effective number of oscillation cycles in the wavelet. The f_0/σ_f was determined[11] as 5 with f_0 ranging from 0.04 to 0.4 Hz[32] in increments of 0.01 Hz. Because the dynamic baroreflex function was well characterized by the transfer function up to around 0.4 Hz based on the corner frequency and slope of gain change,[15,32] the upper frequency limit for analysis was set at 0.4 Hz, considering also the limitation of the step input (low power in high frequency components) and the respiratory frequency of 0.6 Hz. The wavelet duration ($2\sigma_t$) is 39.8 s at 0.04 Hz and 3.98 s at 0.4 Hz, and the spectral band width ($2\sigma_f$) is 0.016 Hz at 0.04 Hz and 0.16 Hz at 0.4 Hz.

The linear trend was subtracted only in animal study, and the continuous wavelet transform of time series $u(t)$ was calculated as the convolution of a complex wavelet [$w(t, f_0)$] with the $u(t)$:

$$\tilde{u}(t, f_0) = w(t, f_0) * u(t) \qquad (2)$$

The power $P(t, f_0)$ of the signal in a frequency band at around f_0 is the squared norm of the wavelet transform: $P(t, f_0) = |\tilde{u}(t, f_0)|^2$. The symbol (*) shows the convolution in the time domain

To identify the dynamic baroreflex property from time-sequential data, we define the transfer function [$H(t, f_0)$] from input to output using wavelet transform as follows.

$$H(t, f_0) = \frac{P_{xy}(t, f_0)}{P_{xx}(t_{\text{event}}, f_0)} \qquad (3)$$

where

$$\begin{cases} P_{xx}(t_{\text{event}}, f_0) = \tilde{x}(t_{\text{event}}, f_0) \cdot \tilde{x}^{\oplus}(t_{\text{event}}, f_0) \\ P_{xy}(t, f_0) = \tilde{x}(t_{\text{event}}, f_0) \cdot \tilde{y}^{\oplus}(t, f_0) \end{cases}$$

$P_{xx}(t_{\text{event}}, f_0)$ is the auto-wavelet spectrum of the input signal [$x(t)$] with central frequency f_0 at a fixed time t_{event} when the power is maximum. The t_{event} shows the sole value of the analysis time (t) at f_0; the transfer function shows the effect of the maximum input power at t_{event} on the output responses during analysis time, t, for every f_0. Here, we used the fixed input value to extract the dynamics strictly against the step input. The cross-wavelet spectrum, $P_{xy}(t, f_0)$, which is an effective way to detect large-amplitude time-localized events,[26] is the convolution of the wavelet transform values of the input-output signals [$\tilde{x}(t_{\text{event}}, f_0)$ and $\tilde{y}^{\oplus}(t, f_0)$]. $\tilde{x}^{\oplus}(t_{\text{event}}, f_0)$ and $\tilde{y}^{\oplus}(t, f_0)$ is the complex conjugate of $x(t_{\text{event}}, f_0)$ and $y(t, f_0)$. The segment for wavelet transform analysis was set at ±30 s of the time of the step input change and was moved to the next area of the step input. The symbol (·) shows the product in the frequency domain, which corresponds to the convolution in the time domain.

To visualize the time-series transfer function during the analysis time (t), the dynamic gain $[|H(t, f_0)| = \sqrt{H_{\text{Re}}(t, f_0)^2 + H_{\text{Im}}(t, f_0)^2}$, where $H_{\text{Re}}(t, f_0)$ and $H_{\text{Im}}(t, f_0)$ are the real and imaginary parts of $H(t, f_0)$] and phase $\left[\varphi(t, f_0) = \tan^{-1}\frac{H_{\text{Im}}(t, f_0)}{H_{\text{Re}}(t, f_0)}\right]$ of the transient transfer function during analysis time were calculated from Eq. (3).

Next, we constructed the bode plot using the maximum dynamic gains, which reflects the maximum values of input and output powers. The phase of Eq. (3) is based on the maximum $P_{xx}(t_{\text{event}}, f_0)$ as the auto-wavelet spectrum of the input signal without the lag time of system response. To calculate the phase of the bode plot, we estimated the lag time of the system response as follows:

$$\hat{L} = t_{Pxy\max} - t_{Pxx\max}, \qquad (4)$$

where $\hat{L}$ is the mean value between 0.35 and 0.4 Hz of f_0. The data between 0.35 and 0.4 Hz (5 points) were averaged because of the varied estimation. The analysis time was set to 0–6 s and the phase unwrap process to make it continuous across 2π phase discontinuities by adding multiples of $\pm 2\pi$ was applied. $t_{Pxx\max}$ is the time at the maximum auto power spectrum of the input data; $t_{Pxy\max}$ is the time at the maximum cross power spectrum of input-output data. Using the estimated lag time (L) of the system response, the phase [$\varphi(t_{\max}, f_0)$] of the transient transfer function is shown as follows:

$$\varphi(t_{\max}, f_0) = \tan^{-1}\frac{H'_{\text{Im}}(t_{\max}, f_0)}{H'_{\text{Re}}(t_{\max}, f_0)} \qquad (5)$$

where

$$H'(t_{\max}, f_0) = H(t_{\max}, f_0) \cdot \exp(-2\pi f_0 iL)$$

$H'_{Re}(t_{max}, f_0)$ and $H'_{Im}(t_{max}, f_0)$ are the real and imaginary parts of $H'(t_{max}, f_0)$ with lag time, L. t_{max} is the time when the dynamic gain is maximum.

Static Characteristics

After the RSNA, AP, and HR during the last 10 s of each CSP level were averaged using the data of the step-input protocol, the static characteristics of total baroreflex loop, neural arc, and cardiac baroreflex control were examined by regression analysis for the logistic function.[24,46,47] To quantify static characteristics of the peripheral arc, linear regression analysis was performed. The closed-loop operating point of the baroreflex (AP_{OP}) was determined from the intersection point between the CSP-AP curve (total baroreflex loop) and CSP-AP identity line. AP_{OP} was also determined from AP at the intersection point between the CSP-RSNA curve (neural arc) and RSNA-AP line (peripheral arc) in the equilibrium diagram.[18]

Standard Analysis

The STFFT as a traditional time-frequency method was applied to the step-input (±20 mmHg) protocol, using the model response between CSP and AP (see Appendix). The time window was set to 12.8 s (64 data points) and 51.2 s (256 points, which is close to that at the lowest frequency in the used wavelet method). After the application of the detrend and Hanning window, power spectral densities of the CSP and AP and the transfer gain of the cross-spectra were computed every 200 ms. In the STFFT (256 points), pseudo-random noises were added to the input (within ±0.1 mmHg) and output (±1 mmHg every 200 ms) signals. The STFFT analysis was also compared with the proposed wavelet analysis over frequencies under the pseudo-random noise within ±0.1 mmHg in the input and ±1 or ±2 mmHg in output every 200 ms.

Experiment of Bezold-Jarisch Reflex

To elucidate the modified wavelet-based analysis in the pathophysiological condition, the previous datasets assessing static baroreflex during BJR[18] were reanalyzed; the data at sampling rate of 200 Hz were averaged every 40 points. In 8 anesthetized rabbits with sectioned aortic depressor nerves, intact vagi, and isolated carotid sinuses, CSP was increased stepwise while AP and HR were recorded before and after 7-min administration of a serotonin ($5\text{-}HT_3$) receptor agonist, phenylbiguanide (PBG, 100 μg/kg/min, intravenous infusion): Control and PBG conditions. Vagal afferent was confirmed as the main pathway of the BJR induced by intravenous PBG infusion.[20]

Cardiac Baroreflex

The role of cardiac baroreflex (CSP to HR response) was studied, focusing on the contribution of the cardiac sympathovagal activity to dynamic baroreflex for AP regulation. The ratio of the transfer functions between cardiac baroreflex and total (CSP-AP) loop was calculated under Control and PBG conditions, using the results from the proposed analysis.

Statistical Analysis

All data are expressed as mean ± SEM. The gain, power, and frequency in the figures are shown in log scales. The transfer functions in the neural and peripheral arcs were normalized in each animal so that the average gain in all stepwise changes of normal condition became unity at 0.04 Hz. To test the difference among six stepwise changes or between the Control and PBG conditions, we obtained the gain at 0.04 ($G_{0.04}$), the average slope of the gains between 0.1 to 0.4 Hz (Slope), and the lag time in each animal. One-way analysis of variance with multiple comparisons using Bonferroni correction[9] was applied to assess the level differences. Differences were considered statistically significant at $p < 0.05$.

Simulation for Closed-Loop Baroreflex

The carotid sinus open-loop animal experiment should be linked to human closed-loop baroreflex to explore the possibility of applying the proposed analysis to clinical diagnosis. We performed a simulation study, using the emulated cardiac baroreflex model from observed AP input to observed HR output under the closed-loop AP response (see Appendix) to test the accuracy of the proposed wavelet-based analysis and to acquire the transfer functions of the cardiac baroreflex for use in human laboratory test.

RESULTS

Test of Wavelet Analysis

The proposed wavelet-based analysis was tested using the baroreflex model response between CSP and AP under carotid sinus open-loop condition (see Appendix). After the calculation of the wavelet power spectrum for the input and the input-output cross spectrum (Fig. 2a), the transfer function was acquired (Fig. 2b). The gains reached the maximum immediately after the step input at 60 s and the phase changed greatly when approaching the maximum gain. Bode plots were extracted from the maximum points of the time-course transfer function with and without

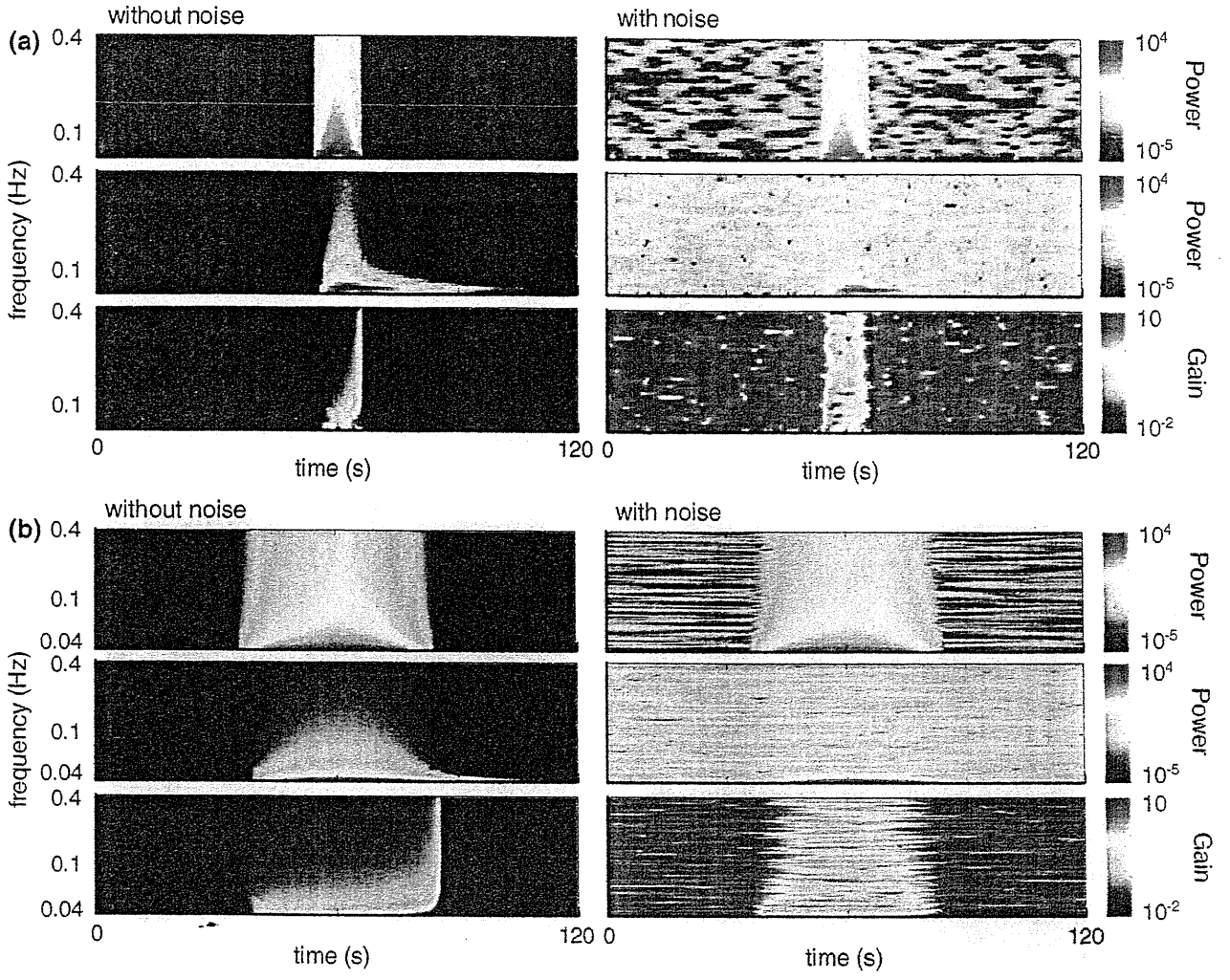

FIGURE 1. Time-frequency method based on the short-time FFT for system identification using the simulated step-input protocol. Time windows, 12.8 s (a) and 51.2 s (b). Power spectral densities of carotid sinus pressure (CSP) input (*top*) and arterial pressure (AP) output (*middle*) and transfer gain (*bottom*) in the absence (*left*) or presence (*right*) of pseudo-random noises.

background noise (Fig. 2c). In the presence of pseudo-random noise (within ±0.01 mmHg in input and ±1 mmHg in output changed every 200 ms), the transfer function closely resembled the theoretical values. Compared to the STFFT (Fig. 1), the proposed wavelet method could accurately estimate the transfer function over different frequencies, regardless of a poor signal to noise (S/N) ratio at higher frequency, because of the property of the step input power (Fig. 2d).

Dynamic Baroreflex

The averaged RSNA, AP, and HR responses to the step-input changes were decreased with the increments in CSP from 40 to 160 mmHg every minute ($n = 8$, Fig. 3a). In the averaged time series ($n = 8$, Fig. 3b), the power spectrums at all step inputs were the same values at each frequency level because of a constant change of +20 mmHg (greater in low frequency and smaller in high frequency). The powers of RSNA, AP, and HR change were higher at CSP_{80-100} than other CSP changes over all frequency ranges, and the magnitudes were especially small at low or high CSP changes.

The averaged ($n = 8$) time series of transfer functions in the neural arc (a), peripheral arc (b), total loop (c) and cardiac baroreflex (d) were calculated after wavelet transform (Fig. 4). In the neural arc, gain values in low frequencies were much less at CSP changes away from the operating point. In the peripheral arc, low pass characteristics in the gains were observed at all CSP changes except the lowest CSP_{40-60} change reflecting spontaneous neural firing. In the total baroreflex loop, the gains at CSP changes within 60–120 mmHg were higher than those at other CSP changes, indicating low-pass characteristics. In the cardiac baroreflex, the gains were smaller at the

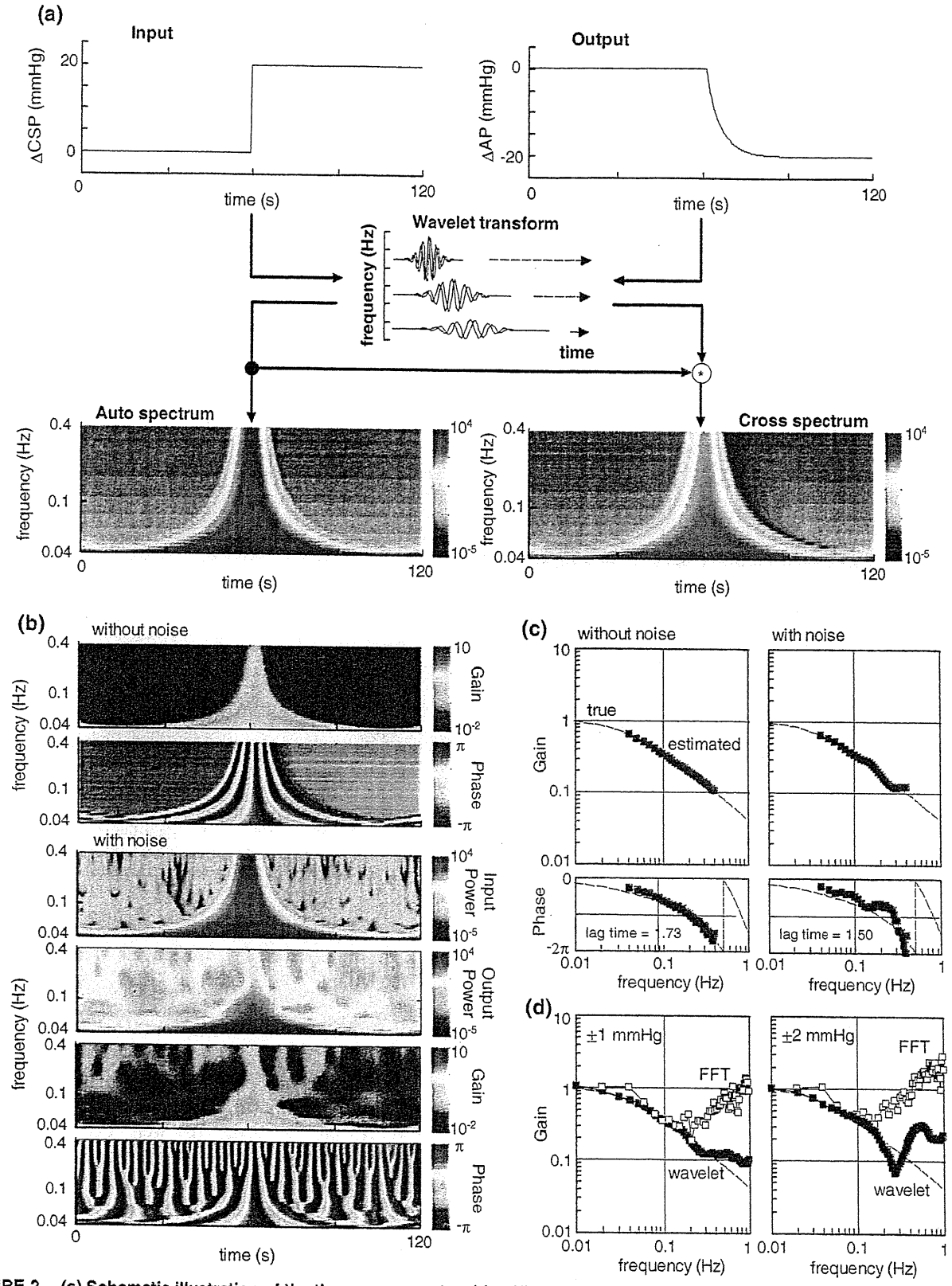

FIGURE 2. (a) Schematic illustration of the time-course system identification using wavelet analysis. The model response of total loop from CSP to AP under the carotid sinus open-loop condition was assessed for 120 s. Step input change of 20 mmHg was added to the system at 60 s. The time-series transfer function estimated by our wavelet analysis (b) and transfer function extracted from the time-course data of the total loop transfer function and the theoretical data (c). Gain (*top*) and phase (*bottom*) in the absence or presence of pseudo-random noise. (d) Gains in the short-time FFT and proposed wavelet analyses over wide frequencies (0.01–1 Hz) under the pseudo-random noise [±1 mmHg (*left*) and ±2 mmHg (*right*)].

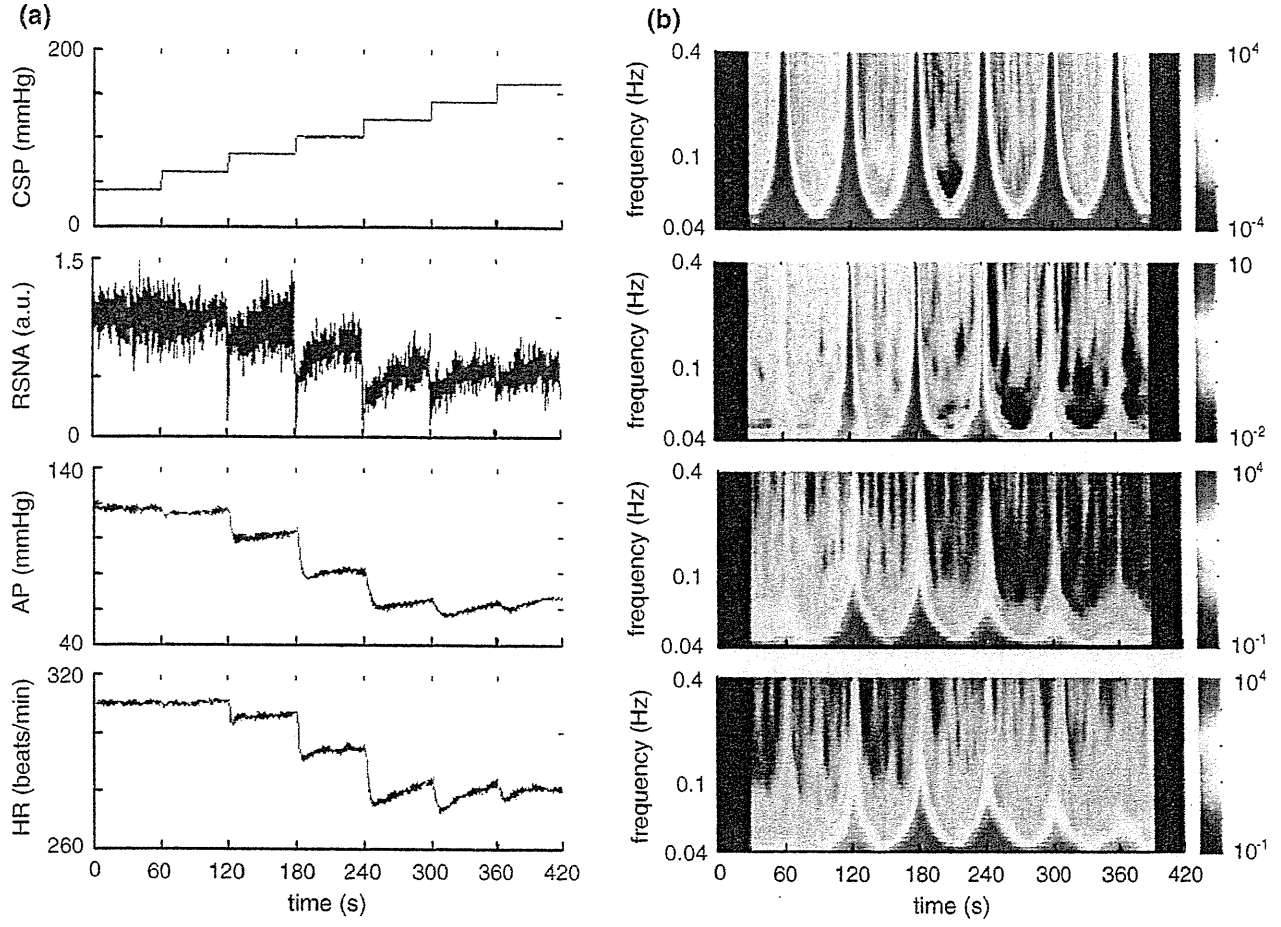

FIGURE 3. Averaged time series (a, $n = 8$) and wavelet power (b, $n = 8$) of CSP, renal sympathetic nerve activities (RSNA), AP, and heart rate (HR) during the static protocol. CSP was increased from 40 to 160 mmHg in 20 mmHg increments, resulting in changes of RSNA, AP, and HR through the carotid sinus baroreflex.

CSP_{40-60} and $CSP_{140-160}$ changes than other CSP changes.

Figure 5 and Table 1 show the average gain and phase ($n = 8$) in the neural arc (a), peripheral arc (b), total loop (c), and cardiac baroreflex (d). In the neural arc, $G_{0.04}$ (2.42 ± 0.07 a.u./mmHg) at the CSP_{80-100} change was the highest among all CSP changes, and was almost four to five times higher than those at the CSP_{40-60} (0.54 ± 0.09, $p < 0.01$) and $CSP_{140-160}$ (0.62 ± 0.06, $p < 0.01$) changes. Slopes increased significantly at lower and higher CSP changes compared with the $CSP_{100-120}$ change. Lag time at CSP_{80-100} was the shortest among all CSP changes. In the peripheral arc, Slope and lag time did not differ significantly among the CSP changes, whereas $G_{0.04}$ showed a tendency to decrease slightly with increase of CSP. In the total baroreflex, $G_{0.04}$ at CSP_{80-100} change (1.28 ± 0.12) was significantly higher compared to other CSP changes. Slopes were significantly greater at CSP changes within 60–120 mmHg than other CSP changes. Lag time did not differ significantly among CSP changes. In the cardiac baroreflex, $G_{0.04}$ (0.90 ± 0.18 and 0.92 ± 0.19 beats/min/mmHg) and Slopes were significantly higher at CSP_{80-100} and $CSP_{100-120}$ changes than other CSP changes. There were no significant differences in lag time among CSP changes.

Static Baroreflex

The static characteristics of the total loop were averaged ($n = 8$). Regression analysis was performed for logistic functions. Response range, coefficient of gain, midpoint of input axis, and minimum value of output were 0.45, 0.11, 99.6, and 0.55 in the neural arc, 65.2, 0.07, 97.6, and 69.4 in the total loop, and 29.5, 0.11, 98.2, and 281.2 in the cardiac baroreflex. Linear regression analysis was performed in the peripheral arc (static gain = 0.0086 and offset pressure = 0.027). The intersection between the CSP-AP curve and the line of identity corresponds to AP_{OP} (94.3 mmHg) located in the steepest portion (80–100 mmHg) of the sigmoid

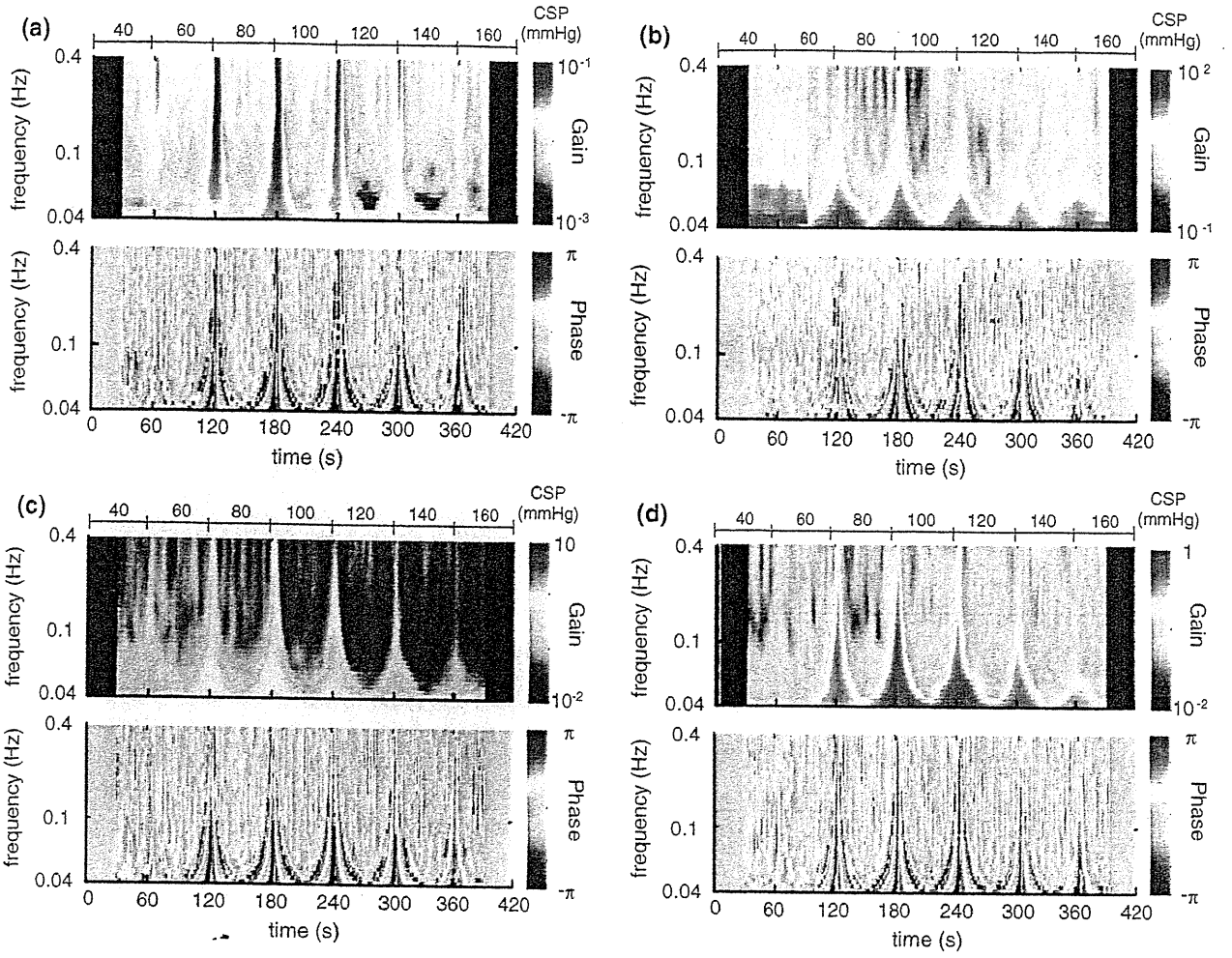

FIGURE 4. Time course of transfer functions of the neural arc from CSP to RSNA (a), peripheral arc from RSNA to AP (b), total baroreflex loop from CSP to AP (c), and cardiac baroreflex from CSP to HR (d) averaged across all animals (n = 8).

curve. In the equilibrium diagram, RSNA decreased with increasing CSP in the neural arc, AP increased with increasing RSNA in the peripheral arc, and the intersection between the two arcs provided the AP_{OP} (99.7 mmHg). In the cardiac baroreflex, HR decreased with the increase in CSP.

Bezold-Jarisch Reflex

In the total loop and cardiac baroreflex, the gains at various CSP changes during the BJR were identified (n = 8, Fig. 6 and Table 2). Averages of gain and phase (Fig. 6d) were derived from the time series in Figs. 6b and 6c. At middle CSP change of the total loop, $G_{0.04}$ was approximately halved under PBG condition compared to Control (0.59 ± 0.09 vs. 1.39 ± 0.15, $p < 0.01$). Slope and lag time did not differ significantly between the PBG and Control conditions at all CSP changes. In the cardiac baroreflex (Fig. 6e), $G_{0.04}$ tended to modulate under PBG condition at low and high CSP changes, but did not differ significantly between the two conditions at middle CSP changes. Slope differed significantly between the two conditions at low CSP change whereas lag time did not differ significantly at all CSP changes.

Cardiac Baroreflex

The ratio of the cardiac baroreflex to the total loop in dynamic characteristics was studied (Fig. 7). For CSP changes within 60–120 mmHg under Control condition, the ratios were almost linear and increased slightly with increase in frequency; in lower or higher CSP changes, they were modulated especially around 0.2 Hz. For CSP changes under PBG condition, overall the ratios were higher than those under Control condition. For CSP changes within 80–120 mmHg under PBG condition, the ratios were almost linear and the slopes were greater than those of Control condition; in lower or higher CSP changes, they

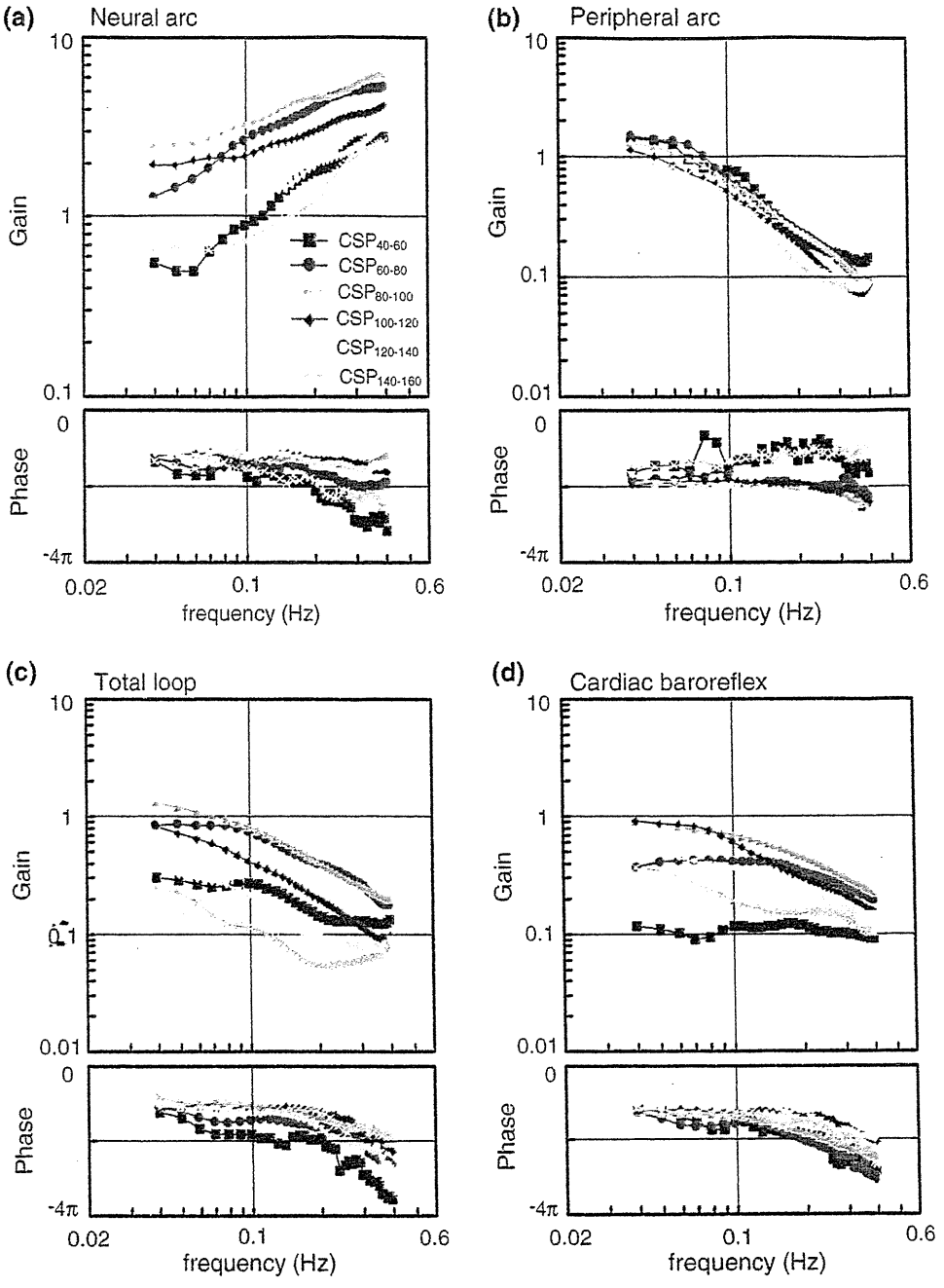

FIGURE 5. Transfer functions of the neural arc from CSP to RSNA, effective peripheral arc from RSNA to AP, total baroreflex loop from CSP to AP, and cardiac baroreflex estimated by wavelet analysis. Average (n = 8) gain (*top*) and phase (*bottom*).

increased within the 0.1–0.2 Hz range and decreased at higher frequencies. The phase difference did not differ among CSP changes under both Control and PBG conditions.

Closed-Loop Baroreflex

Simulation was performed using a cardiac baroreflex system from closed-loop AP input to HR output (Fig. 8a). To test the proposed wavelet analysis, an external disturbance to AP (AP_{noise} = +20 mmHg) was added to the system, and HR responses under carotid sinus open- and closed-loop AP responses were calculated (Fig. 8b). The observed AP and HR (AP_{change} and HR_{change}) were modulated by closed-loop regulation of AP. The CSP is identical with the observed AP_{change}. Gain and phase in the time series (Fig. 8c) and extracted (Fig. 8d) transfer functions were accurately estimated under open and closed AP responses.

TABLE 1. Parameters of the transfer functions in the neural arc, peripheral arc, total loop, and cardiac baroreflex at various step pressure inputs.

	CSP (mmHg)					
	40–60	60–80	80–100	100–120	120–140	140–160
Neural arc						
$G_{0.04}$ (a.u./mmHg)	0.54 ± 0.09	1.25 ± 0.17**	2.42 ± 0.07**,††	1.89 ± 0.13**,†	1.18 ± 0.20*,‡‡,¶¶	0.62 ± 0.06†,‡‡,¶¶
Slope (dB/decade)	17.9 ± 4.1	10.0 ± 1.9	7.7 ± 2.0	5.8 ± 3.1*	11.0 ± 1.8	16.8 ± 3.1¶
Lag time (s)	2.63 ± 0.58	0.78 ± 0.16*	0.27 ± 0.18**	0.48 ± 0.14**	0.45 ± 0.17**	1.83 ± 0.71
Peripheral arc						
$G_{0.04}$ (mmHg/a.u.)	1.42 ± 0.17	1.50 ± 0.18	1.30 ± 0.08	1.13 ± 0.13	0.85 ± 0.10†	0.92 ± 0.09†
Slope (dB/decade)	−24.6 ± 3.3	−29.4 ± 1.3	−28.2 ± 0.8	−26.6 ± 2.8	−22.7 ± 2.8	−23.2 ± 4.6
Lag time (s)	0.40 ± 0.79	1.29 ± 0.20	1.35 ± 0.20	1.35 ± 0.58	2.10 ± 0.69	0.08 ± 0.64
Total loop						
$G_{0.04}$	0.29 ± 0.05	0.85 ± 0.16**	1.28 ± 0.12**,††	0.83 ± 0.09**,‡‡	0.38 ± 0.07††,‡‡,¶¶	0.24 ± 0.04††,‡‡,¶¶
Slope (dB/decade)	−6.8 ± 4.1	−19.4 ± 2.4**	−20.5 ± 1.6**	−20.7 ± 2.1**	−11.8 ± 2.7	−6.4 ± 4.1††,‡‡,¶¶
Lag time (s)	3.03 ± 0.61	2.07 ± 0.12	1.62 ± 0.20	1.82 ± 0.60	2.54 ± 0.62	1.91 ± 0.41
Cardiac baroreflex						
$G_{0.04}$ (beats/min/mmHg)	0.11 ± 0.02	0.37 ± 0.11	0.90 ± 0.18**,††	0.92 ± 0.19**,††	0.55 ± 0.12**,‡,¶	0.36 ± 0.09‡‡,¶¶
Slope (dB/decade)	−2.3 ± 2.1	−10.7 ± 2.3	−15.9 ± 2.8**	−19.0 ± 2.9**	−11.8 ± 2.6	−6.3 ± 3.1‡,¶¶
Lag time (s)	2.13 ± 0.62	2.26 ± 0.34	2.17 ± 0.62	1.51 ± 0.16	1.70 ± 0.61	1.92 ± 0.86

$G_{0.04}$, transfer gain at 0.04 Hz. Slope, average slope of transfer gain between 0.1 and 0.4 Hz.
$p < 0.01$; ** vs. 40–60, †† vs. 60–80, ‡‡ vs. 80–100, and ¶¶ vs. 100–120 mmHg in CSP change; the same symbols of a single show $p < 0.05$.

DISCUSSION

We have shown that the analysis using wavelet transform can identify the dynamic baroreflex properties at various pressure levels from the time-course data under normal (Fig. 5) and pathophysiological conditions (Fig. 6) with background noise. The results of the proposed analysis applied in animal experiments indicate the possibility of its use in the assessment of human baroreflex (Figs. 7 and 8).

Time-Series Analysis for Dynamic Baroreflex

Under the background noise added to the response model, the proposed analysis applied to step response was able to detect the dynamic baroreflex characteristics (Fig. 2). The standard spectral analysis under stationary conditions has high reliability in the baroreflex test, and uses longer data to cancel the noise[31,38] at various pressure inputs and lose the short-term and important changes. In direct calculation of the dynamic characteristics from the step input output data, the traditional time series analysis might also have a disadvantage under noise contamination, which may cause poor S/N ratio in the impaired baroreflex function of cardiac diseases.[41] The STFFT using time windows of a constant range for all frequencies was actually unable to catch the dynamic property especially at higher frequencies under such condition (Figs. 1 and 2d) because of the average one within the whole time window. On the other hand, the modified wavelet-based analysis with improved temporal resolution at higher frequencies to reasonably catch the localized changes in cardiovascular control[4,50] will be effective for extracting the dynamic baroreflex characteristics under nonstationary hemodynamics with a low S/N ratio. Because the baroreflex test may depend on the various S/N ratios depending on the system input (e.g. amplitude) and/or the background noises, further investigations will be required in this regard.

Burgess *et al.*[2] showed that cross spectrum analysis using wavelet transform characterized strong coupling between sympathetic nerve traffic and AP at frequencies of <0.1 Hz. Davrath *et al.*[4] reported that time-varying power obtained from wavelet transform of the spontaneous HR or AP fluctuation in humans are remarkably modulated at approximately 0.1 Hz under standing condition. Whereas the traditional wavelet analysis could extract the localized characteristics of time-series data in a nonstationary condition,[2,4] application to dynamic system identification is difficult because of the limitation in phase extraction. When the same time window is set for the input and output data, the actual information of phase and gain may be lost or split, instead of high temporal resolution of wavelet transform.[34] To apply wavelet analysis to the baroreflex system identification, we expanded the basic analysis by acquiring the transfer function from maximum input and output data. The proposed method was able to acquire the system identification of baroreflex because of the specific characteristics of wavelet